ORIGINAL RESEARCH

American Heart Association | American Stroke Association

hERG Potassium Channel Blockade by the HCN Channel Inhibitor Bradycardic Agent Ivabradine

Dario Melgari, MSc; Kieran E. Brack, PhD; Chuan Zhang, BSc; Yihong Zhang, PhD; Aziza El Harchi, PhD; John S. Mitcheson, PhD; Christopher E. Dempsey, PhD; G. André Ng, MBChB, PhD; Jules C. Hancox, PhD, FSB, FBPhS

***Background*—**Ivabradine is a specific bradycardic agent used in coronary artery disease and heart failure, lowering heart rate through inhibition of sinoatrial nodal HCN-channels. This study investigated the propensity of ivabradine to interact with *KCNH2*-encoded human Ether-à-go-go–Related Gene (hERG) potassium channels, which strongly influence ventricular repolarization and susceptibility to torsades de pointes arrhythmia.

***Methods and Results*—**Patch clamp recordings of hERG current (I_{hERG}) were made from hERG expressing cells at 37°C. I_{hERG} was inhibited with an IC_{50} of 2.07 μmol/L for the hERG 1a isoform and 3.31 μmol/L for coexpressed hERG 1a/1b. The voltage and time-dependent characteristics of I_{hERG} block were consistent with preferential gated-state-dependent channel block. Inhibition was partially attenuated by the N588K inactivation-mutant and the S624A pore-helix mutant and was strongly reduced by the Y652A and F656A S6 helix mutants. In docking simulations to a MthK-based homology model of hERG, the 2 aromatic rings of the drug could form multiple π-π interactions with the aromatic side chains of both Y652 and F656. In monophasic action potential (MAP) recordings from guinea-pig Langendorff-perfused hearts, ivabradine delayed ventricular repolarization and produced a steepening of the $MAPD_{90}$ restitution curve.

***Conclusions*—**Ivabradine prolongs ventricular repolarization and alters electrical restitution properties at concentrations relevant to the upper therapeutic range. In absolute terms ivabradine does not discriminate between hERG and HCN channels: it inhibits I_{hERG} with similar potency to that reported for native I_f and HCN channels, with S6 binding determinants resembling those observed for HCN4. These findings may have important implications both clinically and for future bradycardic drug design. **(*J Am Heart Assoc*. 2015;4:e001813 doi: 10.1161/JAHA.115.001813)**

Key Words: bradycardic agent • HCN • HCN4 • hERG • ivabradine • QT interval • repolarization

Ivabradine is a specific bradycardic agent used to reduce heart rate in the treatment of coronary artery disease and heart failure.[1,2] Heart rate is a determinant of cardiac metabolic demand, and elevated rate against a background of coronary artery disease can induce ischemia in affected individuals.[2] Lowering heart rate in this setting increases diastolic time, reducing oxygen demand and wall stress.[2] β-Adrenoceptor inhibitors and calcium channel blockers can reduce rate effectively, but can also be associated with hypotensive and negative inotropic side-effects.[2,3] In contrast, ivabradine reduces the diastolic depolarization rate of sinoatrial node pacemaker cells through the inhibition of Hyperpolarization-activated cyclic-nucleotide gated (HCN)-channel mediated "funny" current, I_f, which results in bradycardia without a concomitant negative inotropic effect.[1–5]

Ivabradine has generally been considered to exhibit a good overall safety profile without significant effect on heart rate corrected QT interval (QT_c).[3,6] Accordingly, ivabradine has been considered to have no "direct" propensity to produce torsades de pointes (TdP) arrhythmia,[3] though as QT interval varies with rate it is recommended that co-administration of this bradycardic agent with known QT-prolonging drugs should be avoided.[3] However, some concerns regarding cardiac safety of ivabradine have recently been raised. In the

From the School of Physiology & Pharmacology (D.M., Y.Z., A.E.H., J.C.H.) and School of Biochemistry (C.E.D.), Medical Sciences Building, Bristol, United Kingdom; Department of Cardiovascular Sciences, Cardiology Group, Glenfield Hospital, University of Leicester, United Kingdom (K.E.B., C.Z., G.A.N.); NIHR Leicester Cardiovascular Biomedical Research Unit, Leicester, United Kingdom (G.A.N.); Department of Cell Physiology and Pharmacology, Maurice Shock Medical Sciences Building, Leicester, United Kingdom (J.S.M.).

Accompanying Data S1, Figures S1, S2 and Tables S1, S2 are available at http://jaha.ahajournals.org/content/4/4/e001813/suppl/DC1

Correspondence to: G. André Ng, MBChB, PhD, Department of Cardiovascular Sciences, Cardiology Group, Glenfield Hospital, University of Leicester, LE3 9QP United Kingdom. E-mail: gan1@le.ac.uk
Jules C. Hancox, PhD, FSB, FBPhS, School of Physiology & Pharmacology, Medical Sciences Building, University Walk, Bristol BS8 1TD, United Kingdom. E-mail: jules.hancox@bristol.ac.uk

Received February 9, 2015; accepted March 13, 2015.

SIGNIFY trial, which focused on patients with stable coronary heart disease without clinical heart failure, ivabradine was associated with an increase in the combined end point of the trial, which included death from all cardiovascular causes and myocardial infarctions that were nonfatal, in patients with limiting symptoms of angina as a result of physical activity.[7] Also, a recently published meta-analysis of 11 clinical trials has concluded that ivabradine treatment is associated with a 15% increase in relative risk of atrial fibrillation, although the underlying mechanism for this is not clear.[8] Additionally, in April 2014, ivabradine was added to the list of "drugs with a conditional risk" of TdP in the "CredibleMeds" database of QT interval–prolonging drugs, with the update stating "There is substantial evidence that ivabradine is associated with TdP when taken with other medicines that prolong the QT interval, diuretics or drugs that block the metabolic breakdown of ivabradine, or electrolyte abnormalities (low potassium or low magnesium), which may be induced by co-administration of diuretics" (https://www.crediblemeds.org/blog/nelfinavir-and-ivabradine-added-list-drugs-avoid/, CredibleMeds®). Recent case reports of TdP with concomitant administration of ivabradine and other drugs highlight a potential for conditional arrhythmia risk with the drug.[9,10]

Virtually all drugs associated with QT_c interval prolongation and TdP share the ability to inhibit the cardiac rapid delayed rectifier potassium current, I_{Kr}, and its recombinant equivalent "hERG" (the protein product of *human Ether-à-go-go–Related* Gene; alternative nomenclature *KCNH2*).[11,12] Ivabradine (3 μmol/L) was reported to have little effect on delayed rectifier K^+ current from rabbit sinoatrial node myocytes.[5] However, other in vitro data have suggested a propensity for ivabradine to delay ventricular repolarization.[13] To our knowledge, there is no published study of whether or not the drug interacts with hERG potassium channels, and the present investigation was conducted to address this issue. The resulting data demonstrate that ivabradine both inhibits hERG with a potency similar to that reported previously for native I_f and cloned HCN channels and, furthermore, at therapeutically relevant levels can produce a delay in ventricular repolarization and changes electrical restitution properties in intact perfused hearts.

Materials and Methods

Whole Heart Studies

Adult male Dunkin Hartley guinea pigs (n=11, 420 to 520 g) were used following ethical approval and in accordance with the UK Animal Scientific Procedure Act (ASPA) 1986, the US National Institute of Health (NIH Publication No. 85-23, revised 1985) guide for the care and use of laboratory animals, and the European Union directive on the protection of animals for scientific research (2010/63/EU).

Wild-Type and Mutant hERG Channel Constructs

The Human Embryonic Kidney (HEK 293) cell line stably expressing wild-type (WT) hERG channels was kindly donated by Prof Craig January.[14] The hERG 1b construct in pcDNA3.1 was donated by Prof Gail Robertson.[15] HEK cells stably expressing the hERG S6 mutant Y652A[16] and transfection with and use of the inactivation mutant N588K and the S6 mutants S624A and F656A were as described previously.[17,18]

Mammalian Cell-Line Maintenance and Transfection

HEK 293 cells stably or transiently expressing hERG constructs were maintained as previously described.[16,19] Cells were plated on small sterilized glass shards in 40-mm Petri dishes after at least 6 hours of incubation at 37°C (5% CO_2). At least 48 hours after plating, cells were transfected with Lipofectamine™ LTX (Invitrogen) following the manufacturer's instructions. The amount of transfected hERG construct DNA varied between 0.2 and 1.0 μg, depending on the level of protein expression and current conductance of each particular hERG channel construct. In the case of hERG 1a/1b, 0.25 μg of hERG 1a was co-transfected with the same amount of hERG 1b as previously described.[20,21] Between 0.5 and 1.0 μg of CD8 was co-transfected as a transfection marker; in order to identify successfully transfected cells, Dynabeads® (Invitrogen) were used. Electrophysiological recording was conducted after at least 24 hours of incubation at 37°C (5% CO_2) to allow the cells to fully recover and to allow sufficient time for hERG construct expression.

Patch Clamp Electrophysiology

For electrophysiological recording of hERG current (I_{hERG}), glass shards containing plated cells were placed in a small recording chamber mounted on an inverted microscope (Nikon Diaphot, USA) and continuously superfused with a preheated (37°C) standard Tyrode's solution containing (in mmol/L): 140 NaCl, 4 KCl, 2.5 $CaCl_2$, 1 $MgCl_2$, 10 glucose, and 5 HEPES (titrated to pH 7.4 with NaOH).[16,19] Patch-pipettes (Schott #8250 glass; A-M Systems Inc, USA) were pulled (Narishige, PP 830) and polished (Narishige, MF 83) to obtain a final resistance between 2 and 4 MΩ. The intracellular solution used to fill the patch-pipettes contained (in mmol/L): 130 KCl, 1 $MgCl_2$, 5 EGTA, 5 MgATP, and 10 HEPES (titrated to pH 7.2 with KOH).[16,19] All hERG currents were recorded with an Axopatch 200B amplifier (Axon Instruments, now Molecular Devices) and a CV-4/100 or CV203BU headstage. Pipette resistance compensation was between 70% and 80%. Data acquisition was performed through a Digidata 1320

(Axon Instruments, now Molecular Devices). Data digitization rates were 10 to 25 kHz during all protocols and an appropriate bandwidth of 2 to 10 kHz was set on the amplifier.

Langendorff Preparation

Animals were culled by cervical dislocation and the heart was immersion in cold Tyrode solution with 1000 IU of heparin. The ascending aorta was cannulated with hearts retrogradely perfused in Langendorff mode (20 mL/min) via a Gilson minipulse 3 peristaltic pump (Anachem, Luton, UK). Tyrode solution contained (in mmol/L): Na^+ 138.0; K^+ 4.0; Ca^{2+} 1.8; Mg^{2+} 1.0; HCO_3^- 24; $H_2PO_4^-$ 0.4; Cl^- 124; and glucose 11 (mmol/L), maintained at 37°C and at a pH of 7.4 by constant bubbling with 95% O_2/5% CO_2. A 2-mm-diameter polypropylene catheter (Porlex, Kent, UK) was inserted at the apex of the left ventricle for thebesian venous effluent drainage. Hearts were instrumented to record left ventricular pressure, coronary perfusion pressure, and monophasic action potentials (MAP) at the left ventricle apex and base with MAP contact electrodes (73-0150, Harvard Apparatus, Kent, UK) using a custom made DC-coupled high-input impedance differential amplifier (Joint Biomedical Workshop, University of Leicester, UK). The effect of ivabradine was investigated at 0.1, 0.2, 0.3, 0.4, and 0.5 μmol/L in incremental concentrations, and by measuring MAP duration during constant ventricular pacing and electrical restitution (described in detail in Data S1).

Docking of Ivabradine to a hERG Homology Model

The docking of ivabradine to WT hERG was tested by using a homology model of the hERG channel pore region (pore helix, selectivity filter, and S6 helices) in the open configuration based on the crystal structure of MthK channel,[22] as previously conducted in our laboratory.[16,19,23] Further details of docking simulation methods are given in Data S1.

Data Analysis and Statistics

Details of data analysis including equations used for data fits are given in the Data S1. Statistical analysis and data distribution were tested using Graphpad Prism versions 5.03, 6.0c, and the Kolmogorov–Smirnov normality test. Statistical comparisons were made using paired or unpaired 2-tailed *t* tests, Wilcoxon matched-pairs signed-rank test, and 1-way (repeated measures, where indicated) or 2-way ANOVA, as appropriate. Details of the statistical test used to evaluate significance for results of particular experiments are given alongside the "*P*" values in the "Results" text or in the relevant Table or Figure legend.

Results

Ivabradine Inhibits I_{hERG}

In order to determine the sensitivity of I_{hERG} to ivabradine, I_{hERG} "tail" amplitude was monitored during repetitive application of the protocol shown in the lower panel of Figure 1A.[16,24] Figure 1A shows currents in control and in the presence of 3 μmol/L ivabradine, demonstrating a >50% reduction in I_{hERG} tail amplitude and also a marked reduction in pulse current. Inhibition of I_{hERG} by this concentration of ivabradine developed with a time-constant of 20.7±2.6 seconds (n=5); at a higher concentration of 30 μmol/L I_{hERG} inhibition developed more rapidly with a time-constant of 6.5±0.2 seconds (see Figure S1). Reversibility of block was investigated for 30 μmol/L ivabradine (the highest drug concentration tested); on washout of the drug I_{hERG} recovered to 80.7±3.3% of the control value (see Figure S1). In Figure 1B, mean I_{hERG} tail data for inhibition by 5 ivabradine concentrations are plotted and fitted with a Hill function (equation 2, Data S1), yielding an IC_{50} value of 2.07 μmol/L (CI: 1.80 to 2.37) and Hill slope (n_H) of 0.80 (CI: 0.72 to 0.89). Both fast and slow time-constants of I_{hERG} deactivation (measured on repolarization to −40 mV) were slower in the presence of 3 μmol/L ivabradine than in control (τ_{fast}: 263.3±16.8 ms and 584.9±38.2 ms; $P<0.01$ paired *t* test; τ_{slow}: 1731.0±117.5 ms and 3253.0±388.1 ms; $P<0.001$ paired *t* test; for control and ivabradine, respectively). In additional experiments to simulate hypokalemia (not shown), effects of ivabradine on I_{hERG} inhibition were compared at 2 and 4 mmol/L $[K^+]_e$ (for both 3 and 10 μmol/L ivabradine) and were found not to differ at the 2 $[K^+]_e$ levels. There is evidence that native I_{Kr} channels may comprise heteromeric hERG1 a/1b channels;[15,25,26] consequently, additional concentration-response experiments were performed on co-expressed hERG1 a/1b. The concentration-response relation for ivabradine inhibition of hERG 1a/1b I_{hERG} is also included in Figure 1B, with a derived IC_{50} of 3.31 μmol/L (CI: 2.97 to 3.70); and n_H of 1.06 (CI: 0.93 to 1.19). As the IC_{50} values for hERG 1a and hERG 1a/1b were similar to one another, all subsequent experiments were performed using hERG 1a.

Through the use of depolarizing voltage commands to differing test potentials (see Figure S2 for details), I_{hERG} block by ivabradine was observed to exhibit some voltage dependence: Figure 1C shows a plot of fractional block of I_{hERG} tails against command voltage, with superimposed activation curves in control and 3 μmol/L ivabradine (control $V_{0.5}$ was −18.15±4.05 mV and k was 5.82±0.27; ivabradine $V_{0.5}$ was −23.25±3.35 mV and k was 4.78±0.55 [n=5]; see also Figure S2). The voltage range

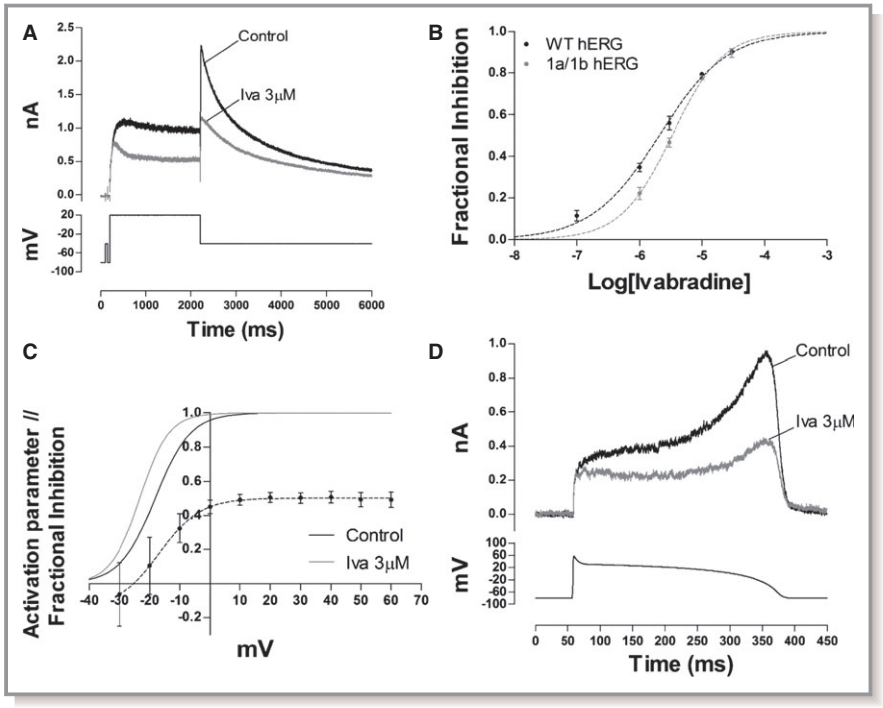

Figure 1. Effect of ivabradine on I_{hERG} and $I_{hERG\text{-}1a/1b}$. A, Upper traces show representative I_{hERG} records elicited by the step protocol shown below, in Control and after the application of 3 μmol/L ivabradine (the voltage protocol was applied at 12-s intervals). The amplitude of peak I_{hERG} tails at −40 mV was measured relative to current elicited by the initial brief 50-ms step from −80 to −40 mV. B, Normalized concentration-response relationship for ivabradine block of I_{hERG} tails for WT hERG 1a and hERG 1a/1b. Fractional inhibition of I_{hERG} tails was assessed at each of 5 ivabradine concentrations for WT 1a and 4 ivabradine concentrations for 1a/1b hERG (n≥5 at each concentration for each expression condition). C, Voltage dependence of ivabradine block (black dotted line) and voltage-dependent activation relations for I_{hERG} in Control (black continuous line) and in the presence of 3 μmol/L ivabradine (gray line). The activation relations were simulated by calculating activation variables at 2-mV intervals using equation 4 in Data S1 and the activation parameters yielded by fitting experimental data (Figure S1). D, Upper traces show representative records of I_{hERG} elicited by the action potential protocol shown below, in Control and after the application of 3 μmol/L ivabradine. hERG indicates human Ether-à-go-go-Related Gene; I_{hERG}, hERG current; WT, wild-type.

over which I_{hERG} tail inhibition exhibited marked voltage dependence coincided closely with the rising phase of the I_{hERG} activation relation, consistent with gating (activation)-dependent block. Figure 1D shows the effect of 3 μmol/L ivabradine under AP voltage clamp: a similar level of peak I_{hERG} block was observed as for the I_{hERG} tail during the conventional protocol shown in Figure 1A. In 5 experiments, peak repolarizing current during the AP command was reduced 52.9±3.1%, which was not significantly different from the I_{hERG} tail reduction under conventional voltage clamp (56.0±3.3%; n=5, unpaired *t* test $P>0.05$). These findings demonstrate that ivabradine induces a concentration-dependent inhibition of hERG channels with an IC_{50} similar to that reported for native I_f and HCN channels (see Table S1).

Ivabradine Delays Ventricular Repolarization in Intact Perfused Hearts

The effects of ivabradine on cardiac repolarization were investigated in the Langendorff perfused guinea pig heart. Ivabradine decreased heart rate in a dose-dependent manner (Table S2). At concentrations >0.5 μmol/L, ivabradine produced sinus arrest with a junctional escape rhythm and therefore the effects of higher concentrations were not investigated.

MAP recorded during constant ventricular pacing at 200-ms cycle length, during control, and 0.2 μmol/L ivabradine (a therapeutically relevant concentration of drug) are illustrated in Figure 2A and 2B. Ivabradine significantly ($P<0.05$; paired *t* test) prolonged MAP duration at both 50% and 90% repolar-

ization at both the apex and base (Figure 2C and 2D, respectively, and Table S2).

Effects of ivabradine on electrical restitution were also examined. Figure 3A shows MAPD-restitution curves measured at the left ventricle base of a typical heart in control conditions and with progressively increasing concentrations of ivabradine (0.1 to 0.5 μmol/L). During ivabradine perfusion, the restitution curve was profoundly altered, with shifts upwards and to the left. Mean maximal $MAPD_{90}$ increased significantly (Table S2) and the mean maximal restitution slope was significantly ($P<0.05$; repeated-measures ANOVA with Bonferroni post hoc test) steepened, but in the basal region only (Figure 3B and 3C). Mean effective refractory period was also significantly ($P<0.05$; repeated measures ANOVA with Bonferroni post hoc test) prolonged during ivabradine perfusion (Table S2). When the interval between the pacing stimulus and S_2-activation was plotted (Figure 3D and 3E), it was evident that ivabradine prolonged S2 delay, indicating a delay in extrastimulus conduction through the left ventricle. At 140 ms S_1 to S_2 interval, S_2 delay was significantly ($P<0.05$; paired *t* test) increased at both apex (20.07±0.47 to 22.05±0.85 ms) and the base (24.57±1.25 to 27.75±1.41 ms) at 0.1 μmol/L ivabradine. These results demonstrate that ivabradine can induce substantial effects on ventricular repolarization and conduction in the intact heart.

Mechanism of I_{hERG} Inhibition: Gating Dependence and Molecular Determinants

The time-dependent gating dependence of I_{hERG} inhibition was pursued through the use of an "envelope of tails" protocol (Figure 4A, bottom of lower panel), with representative traces in control and 3 μmol/L ivabradine shown in upper and lower panels, respectively, of Figure 4A. With short activating pulses during the protocol, comparatively little I_{hERG} block was observed, with block progressively increasing with depolarizing step duration over the first ≈200 ms of the protocol. Figure 4B shows mean normalized data for the time-course of I_{hERG} development during the envelope protocol, while Figure 4C shows the time-course of fractional block of the I_{hERG} tail during the envelope of tails protocol, which was well fitted by a single exponential (equation 5, Data S1) with a time-constant of

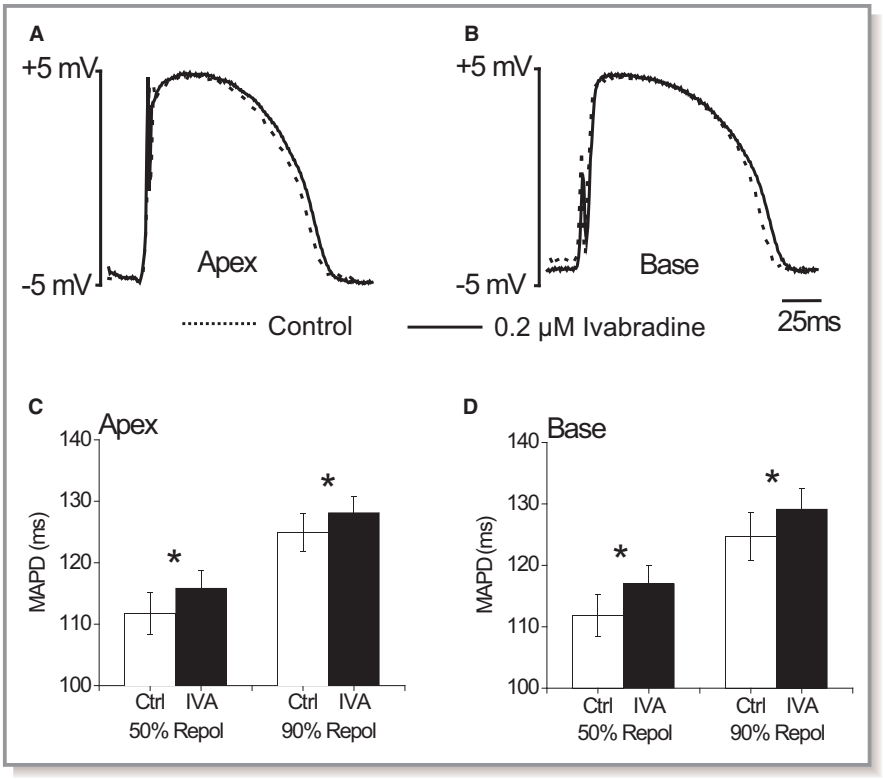

Figure 2. Effect of ivabradine on ventricular monophasic action potential (MAP). A and B, Representative MAPs during Control (dashed line) and 0.2 μmol/L ivabradine (solid line) from Apex (A) and Base (B) of the guinea-pig isolated Langendorff-perfused heart. C and D, MAP duration (MAPD) at 50% repolarization and 90% repolarization during Control and 0.2 μmol/L ivabradine (solid bars) from apex (C) and base (D) (n=7; **P*<0.05, paired *t* test).

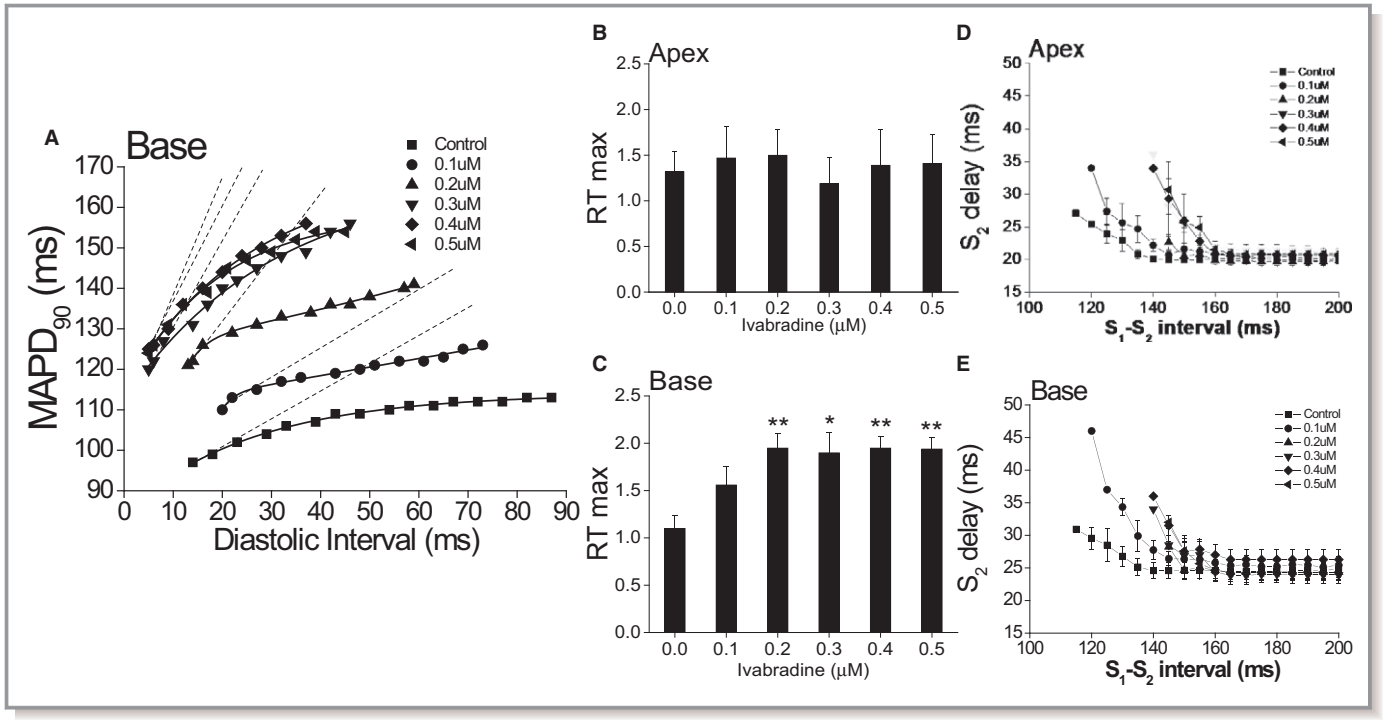

Figure 3. Effect of ivabradine on ventricular electrical restitution. A, Representative example of MAPD-restitution curves at the left ventricular base of an isolated perfused heart during control and at each ivabradine concentration studied (0.1, 0.2, 0.3, 0.4, and 0.5 μmol/L). B and C, Mean data for maximum slope of the restitution curve (RT max) at each ivabradine concentration examined (n=6) at the left ventricular apex (B) and base (C) (**P<0.01 vs Control; *P<0.05 vs Control; repeated measure single-factor ANOVA with Bonferroni post hoc test). D and E, Mean data for S2-delay (duration between the pacing stimulus and S_2-activation) at each ivabradine concentration examined at the left ventricular apex (D) and base (E) (n=7). MAPD indicates monophasic action potential duration.

111.6±21.3 ms (n=5). This indicates strong time-dependence of the drug's inhibitory action during progressively longer periods of gating during the depolarizing command, consistent with rapid open channel block. Figure 5A shows the protocol used to study voltage-dependent availability (inactivation) of I_{hERG} in the absence and presence of ivabradine,[18,27] with representative traces during the second depolarization following the repolarizing ladder of steps, shown in Figure 5B and 5C (selected sweeps). There was a modest shift in I_{hERG} availability (inactivation) with ivabradine. This is illustrated more clearly in Figure 5D, which shows mean normalized availability plots in the absence and the presence of the drug, fitted with equation 6 (Data S1). In control, the inactivation $V_{0.5}$ was −77.6±1.5 mV and k was 21.7±1.9, whereas in ivabradine, the $V_{0.5}$ was −86.8±1.7 mV and k was 23.2±0.4 (n=6). Figure 5E shows plots of the inactivation time-constant at +40 mV, following the brief repolarizing step to −120 mV; inactivation time-course was not significantly altered by ivabradine (n=6; P>0.05 Wilcoxon matched-pairs signed-rank test).

A number of hERG inhibitors (typically, but not exclusively high-affinity inhibitors) are markedly dependent on intact channel inactivation for channel inhibition to occur,[16,28–31] and the −10-mV shift in voltage dependence of inactivation with ivabradine shown in Figure 5 is consistent with some stabilization of the inactivated state in the presence of the drug. Inactivation-dependence of ivabradine inhibition of I_{hERG} was probed further using the N588K attenuated-inactivation mutant.[16,30,31] Figure 6A shows representative traces of N588K I_{hERG} before and during exposure to ivabradine, elicited using the same experimental protocol employed to study WT I_{hERG}, whereas Figure 6B shows the concentration dependence of ivabradine inhibition of N588K I_{hERG}, superimposed on that for the WT channel. The IC_{50} for N588K inhibition was 10.29 μmol/L (CI: 8.73 to 12.15); n_H 0.68 (CI: 0.57 to 0.79), which was ≈5-fold that for WT I_{hERG} . This compares with potency shifts of 12- to 20-fold reported previously for methanesulphonanilide inhibitors (E-4031 and D-sotalol;[31,32]). Collectively, our data indicate gated-state dependence of I_{hERG} block by ivabradine, with inactivation likely contributing to stabilizing drug binding to the channel.

The dependence of ivabradine on canonical drug-binding residues within the I_{hERG} channel pore was probed through the use of alanine mutants of pore helix (S624) and S6 helix (Y652 and F656) residues.[12] Three and 10 μmol/L ivabradine were tested against each mutant (and their corresponding WT control). The results are summarized in Figure 6C through 6F and Table.

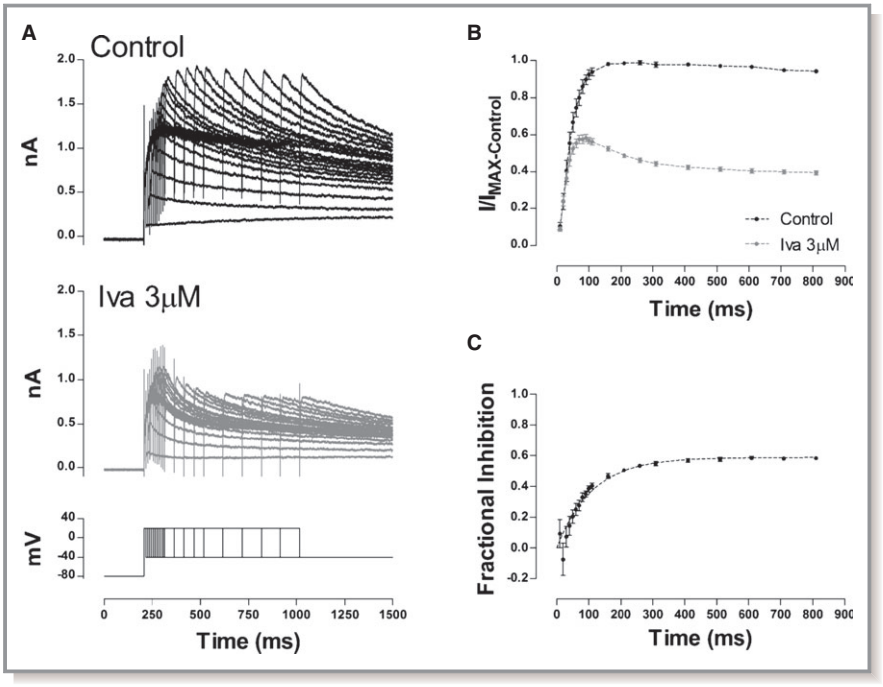

Figure 4. Time dependence of human Ether-à-go-go-Related Gene current (I_{hERG}) inhibition by ivabradine. A, Representative traces of I_{hERG} in Control (upper panel) and in the presence of 3 μmol/L ivabradine (lower panel) elicited by the "envelope of tails" protocol shown at the bottom of the lower panel. B, Time dependence of normalized tail I_{hERG} in Control (black) and in the presence of 3 μmol/L ivabradine (gray) (n=5). Data at each time point were normalized to the maximum tail current elicited by the protocol in Control. Lines connect successive points in each plot. C, Time dependence of fractional block of I_{hERG} by 3 μmol/L ivabradine, fitted with a mono-exponential function (dotted line, equation 5, Data S1) (n=5) to yield τ value in the text.

Figure 6C shows representative traces of S624A I_{hERG} before and during the application of 3 μmol/L ivabradine, elicited by the same protocol used to study WT and N588K hERG. The plots in Figure 6F show mean data for 3 and 10 μmol/L ivabradine. Notably, 10 μmol/L ivabradine inhibited S624A I_{hERG} by 47.5±3.6% (n=6) (close to 50% inhibition), consistent with a ≈5-fold reduction in blocking potency. Figure 6E shows the effects of 3 μmol/L ivabradine on Y652A I_{hERG}, with mean data for 3 and 10 μmol/L ivabradine shown as bar charts in Figure 6F and, numerically, in Table. I_{hERG} block was markedly attenuated for the Y652A mutation. Figure 6D shows comparable data for the F656A mutation, for which I_{hERG} was measured as inward tail current in high (94 mmol/L) $[K^+]_e$ (the voltage step protocol is shown in full above Figure 6F and with the repolarization phase expanded in Figure 6D, lower panel) together with its corresponding WT control (Figure 6D, upper panel). WT I_{hERG} block by 3 and 10 μmol/L ivabradine was moderately reduced for the inward current tail in high $[K^+]_e$, compared to that for outward current tails with the same drug concentrations (Table). This is consistent with some interference between the permeant ion and ivabradine interaction with the channel, under conditions of inward K^+ flux.[16,19] When F656A I_{hERG} was studied under the same conditions, inhibition was markedly attenuated compared to the WT channel (Figure 6D and Table). Thus, I_{hERG} inhibition by ivabradine showed a strong dependence on interactions with canonical S6 aromatic binding residues. This was pursued further through docking simulations to an open state hERG homology model based on MthK channel crystal structure. The 6 best-ranked conformations were selected, and 1 of these is shown in Figure 7. In the majority of the poses yielded by GOLD, the ivabradine molecule tended to lie lower in the pocket defined by Y652 and F656 side chains, closer to the pore mouth and far from the selectivity filter (Figure 7A). The drug orientation was almost horizontal (ie, perpendicular to the K^+ ion permeation path, Figure 7B) with a folded compact conformation. This conformation allowed the 2 aromatic rings to form multiple π-π interactions with the aromatic side chains of both Y652 and F656 (Figure 7C). In addition, a cation-π interaction between the methylene group adjacent to the protonated nitrogen and F656 side chain may also be involved in the drug binding.[33] These results are consistent with the strong reduction of I_{hERG} inhibition observed for both Y652A and F656A hERG mutants (Figure 6).

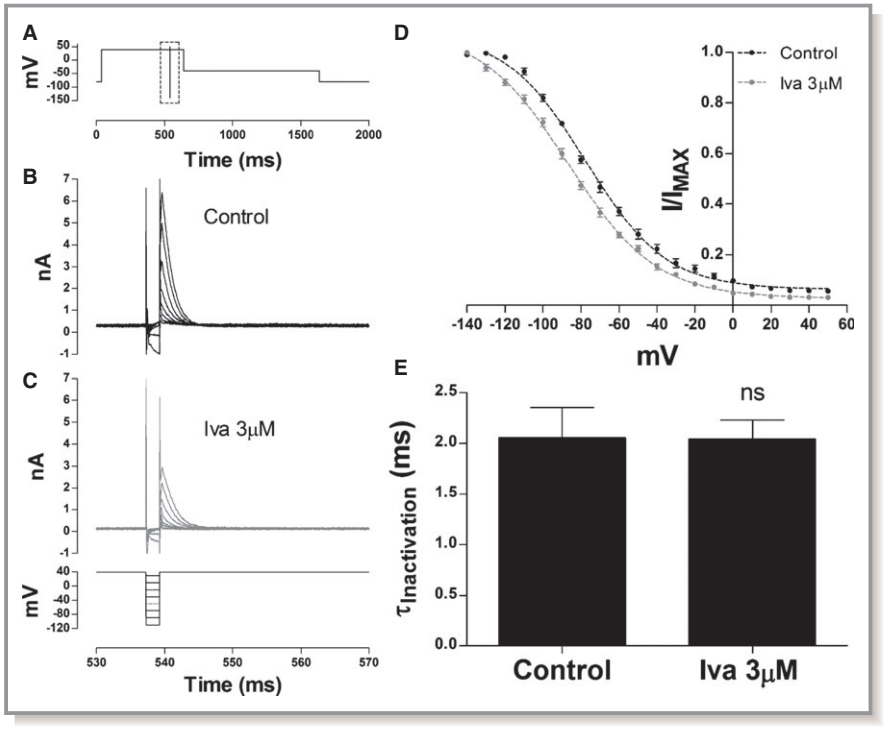

Figure 5. Effect of ivabradine on hERG channel availability. A, Voltage protocol used to study hERG channel availability. B and C, Sample traces of hERG transient current in Control (B) and in the presence of 3 μmol/L ivabradine (C) elicited by the portion of the 3-step protocol shown at the bottom of (C) (expanded from the dashed box in (A). For clarity of display, only selected test voltages are reported, while the full protocol spans from −140 to +50 mV with a 10-mV increase at each step). D, Voltage dependence of the normalized resurgent current elicited by the third step of the 3-step protocol in Control (black) and in the presence of 3 μmol/L ivabradine (gray) (n=6). Experimental data were fitted with equation 6 (dotted lines, Data S1) to give the $V_{0.5}$ and k values in the Results. E, Time constant of I_{hERG} inactivation calculated by fitting the peak transient current at +40 mV after a 2-ms step to −120 mV with a mono-exponential decay function (equation 7, Data S1). The application of 3 μmol/L ivabradine had no significant effect on $\tau_{inactivation}$ (n=6, ns $P>0.05$, Wilcoxon matched-pairs signed-rank test). hERG indicates human Ether-à-go-go-Related Gene; I_{hERG}, current hERG.

Discussion

Results in Context: Ivabradine Effects on Repolarization and hERG

In an early study, 3 μmol/L ivabradine was reported to produce a 14% to 15% prolongation of APD_{50} and APD_{90} of rabbit Purkinje fibers, and an ≈24% reduction in sinoatrial nodal rate.[34] The drug is the *S* stereoisomer of the parent racemate ((±)-S 15544) and, in a direct comparison, its companion *R* stereoisomer was reported to produce a more marked effect on repolarization of both guinea-pig papillary muscles and rabbit Purkinje fibers[35]; only the *R* stereoisomer prolonged the QT_c interval of anesthetized pigs (at intravenous doses of up to 1 mg kg^{-1}).[35] In a more recent in vitro study, ivabradine was reported to produce a modest dose-dependent (0.1 to 10 μmol/L) prolongation of canine ventricular action potential duration (APD), an action that was substantially augmented in the setting of pharmacologically impaired repolarization reserve.[13] In the same study, a high (10 μmol/L) ivabradine concentration produced an ≈11% lengthening of APD_{90} from human ventricular papillary muscle.[13] The effects of the drug on ventricular repolarization in these previous experimental studies largely occurred at concentrations considerably exceeding the plasma concentration range in humans. Thus, when a 30-mg oral dose of ivabradine has been administered to healthy volunteers, a mean maximum plasma level of 0.17 μmol/L has been reported[36] and, in a separate study, multiple dosing with 5 to 20 mg of ivabradine resulted in plasma C_{max} values of 34 to 137 nmol/L.[37] In the present study, ivabradine concentrations (100 to 500 nmol/L) overlapping this range affected $MAPD_{50}$ and $MAPD_{90}$ and effective refractory period in a concentration-dependent fashion, in both apex and base of the guinea-pig left ventricle. It is unclear why the effects of ivabradine seen here are more marked than some previous studies; however, the use

of different species and/or preparations may contribute. For example, the comparatively low sensitivity of human ventricular APs to 1 μmol/L ivabradine was observed in measurements from superfused papillary muscles,[13] whereas a prior study showing small effects of ivabradine on guinea-pig action potentials at concentrations of 1 μmol/L or greater also utilized papillary muscle preparations.[34] Penetration of the drug into these preparations may differ from that in perfused hearts with an intact coronary circulation. Our experiments also showed some potential for apical–basal heterogeneity of effects on restitution. Collectively, our MAP data are consistent with the potential for a direct effect of the drug on ventricular repolarization, effective refractory period, and restitution kinetics at high plasma concentrations, or in a setting of tissue drug accumulation. Steepening of the APD restitution curve has been associated with increased risk of wave-break and oscillation and generation of electrical alternans and fibrillation.[38,39]

Prior studies have produced conflicting data on the effect of ivabradine on repolarizing K^+ currents. Koncz et al reported no significant effect of ivabradine on rabbit ventricular inwardly rectifying K^+ current (I_{K1}) at 10 μmol/L, while suggesting that the drug inhibits rabbit ventricular I_{Kr} with an IC_{50} of ≈3.5 μmol/L.[13] By contrast, Bois et al reported no effect of 3 μmol/L ivabradine on I_K from rabbit sinoatrial cells, with only a small effect at 10 μmol/L.[5] The present study demonstrates unequivocally that ivabradine can inhibit hERG, with an IC_{50} of ≈2 to 3 μmol/L, concordant with an ability to inhibit native I_{Kr}.[13] In absolute terms, the IC_{50} for ivabradine against hERG is lower (ie, potency higher) than for either disopyramide or ranolazine under similar conditions (≈7 to 8 μmol/L[16,19]), both of which inhibit I_{hERG} at clinically relevant antiarrhythmic concentrations. At low plasma ivabradine levels, the "safety margin"[40] for ivabradine use would be >30, consistent with a normally low propensity to produce QT_c prolongation in patients,[6] although at higher levels this would not neces-

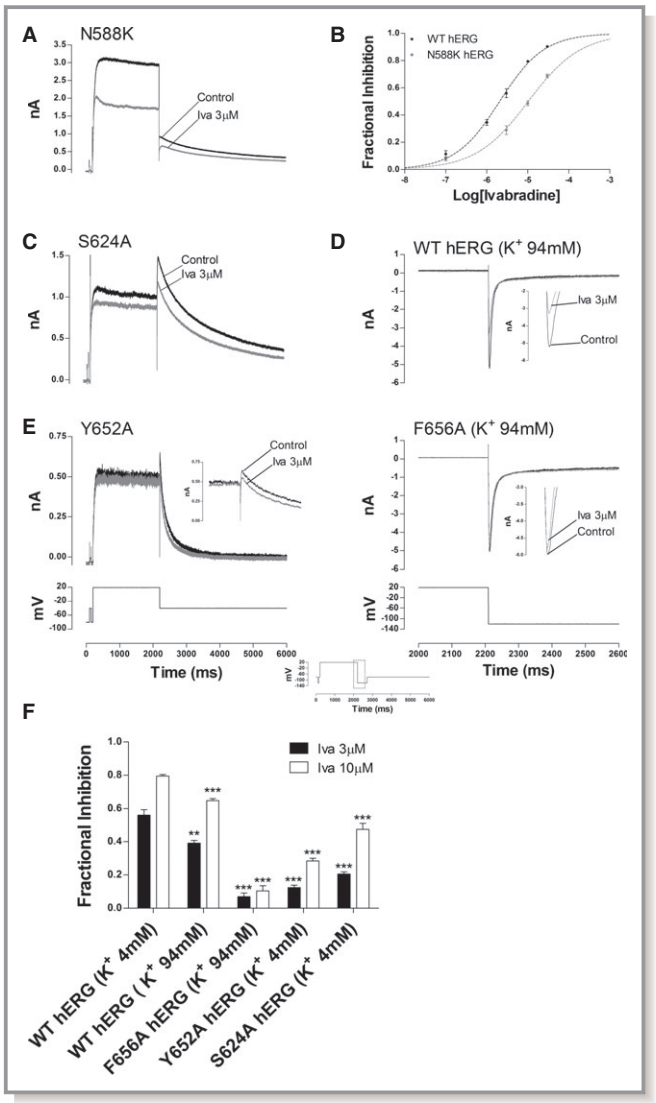

Figure 6. Effect of hERG mutants on ivabradine block of I_{hERG}. A, Representative traces of N588K I_{hERG} elicited by a step protocol identical to that used to study WT I_{hERG} in Figure 1A in control and in the presence of 3 μmol/L ivabradine. B, Concentration response relation for ivabradine action on N588K I_{HERG} compared with that for WT I_{hERG}. Fractional inhibition was assessed for I_{hERG} tails at each of 4 concentrations (n≥5 at each concentration). C, Representative traces of S624A I_{hERG} elicited by same protocol as used to study N588K in control and in the presence of 3 μmol/L ivabradine. D, Voltage protocol with hyperpolarizing step to −120 mV used to elicit WT (upper panel) and F656A (lower panel) inward currents in high (94 mmol/L) external potassium condition is shown as an inset above Figure 6F. The dotted box frames the portion of the protocol shown on an expanded timescale at the bottom of the lower panel. Upper and lower panels each show representative traces in Control and 3 μmol/L ivabradine while the insets to both panels show peak inward currents on expanded scale for clarity of display. E, Representative traces for Y652A I_{hERG} elicited by same protocol as used to study N588K and S624A hERG, in Control and in the presence of 3 μmol/L ivabradine. The inset shows tail currents on an expanded timescale in order to aid visualization of the peak I_{hERG} tail in control and drug. F, Bar charts that summarize the effect of 3 (black bars) and 10 μmol/L (white bars) ivabradine on WT I_{hERG} in standard (4 mmol/L) external potassium condition elicited at −40 mV by a standard outward I_{hERG} protocol (n=5 for 3 μmol/L and n=6 for 10 μmol/L), on inward WT I_{hERG} elicited at −120 mV in high (94 mmol/L) external potassium condition (n=5 for both concentrations), on F656A inward current elicited at −120 mV in high potassium condition (n=5 for both concentrations) and on S624A and Y652A outward current elicited at −40 mV in standard external potassium condition (n≥5 at each concentration) (**P<0.01 against respective Control, ***P<0.0001 against respective Controls; for details of tests used see legend to Table). hERG indicates human Ether-à-go-go-Related Gene; I_{hERG}, current hERG; WT, wild-type.

Table. Fractional Inhibition of WT and S6 and Pore Helix Mutant (Y652A, F656A, and S624A) I_{hERG} by 3 and 10 μmol/L Ivabradine

Channel	Fractional Inhibition (%)	
	Ivabradine 3 μmol/L	Ivabradine 10 μmol/L
WT hERG ($[K^+]_e$ of 4 mmol/L)	56.0±3.3 (5)	79.5±0.9 (6)
S624A hERG ($[K^+]_e$ of 4 mmol/L)	20.6±1.2 (6) ***	47.5±3.6 (6) ***
Y652A hERG ($[K^+]_e$ of 4 mmol/L)	12.4±1.5 (6) ***	28.4±1.7 (6) ***
WT hERG ($[K^+]_e$ of 94 mmol/L)	39.1±1.6 (5) **	64.8±1.3 (5) ***
F656A hERG ($[K^+]_e$ of 94 mmol/L)	7.05±2.2 (5) ***	10.5±3.1 (5) ***

Data are presented as mean±SEM. Numbers in parentheses next to fractional block percentages denote number of replicates (N value). WT hERG with a $[K+]_e$ of 4 mmol/L was the control for S624A and Y652A hERG (all assessed using the standard voltage protocol shown in Figure 1; ***P<0.0001 vs WT, 1 way ANOVA with Dunnett's post-test). WT I_{hERG} with a $[K+]_e$ of 94 mmol/L was the control for F656A hERG (both assessed using inward I_{hERG} tails in high $[K+]_e$, see Figure 6; ***P<0.0001 for F656A vs its WT control; unpaired t test). Inhibition of WT I_{hERG} at 4 and 94 mmol/L $[K+]_e$, assessed respectively through measurement of outward and inward I_{hERG} tails, were compared with one another using an unpaired t test (**P<0.01; ***P<0.0001 at 3 and 10 μmol/L, respectively, shown for "WT hERG ($[K+]_e$ of 94 mmol/L)"). hERG indicates human Ether-à-go-go-Related Gene; I_{hERG}, current hERG; WT, wild-type.

sarily be the case: safety margin values of 15 and 24 (for a C_{max} of 137 nmol/L and hERG IC_{50} values of 2.07 μmol/L and of 3.31 μmol/L) can be calculated for hERG 1a and hERG 1a/1b, respectively. It is worth noting that although the IC_{50} values for hERG 1a and hERG 1a/1b observed in this study are similar, the differences between ivabradine block in the two expression conditions are greatest for lower concentrations (Figure 1), relevant to normal serum concentrations in patients. As human I_{Kr} has been proposed to comprise hERG 1a/1b,[41] this may explain the normally low risk of QT_c prolongation/TdP when ivabradine is given in the absence of other risk factors for QT_c prolongation/TdP.

Considered together, our hERG and MAPD data are suggestive that co-administration of ivabradine with drugs known to prolong the QT interval should be approached with caution not merely because ivabradine-induced bradycardia could exacerbate effects of other drugs on repolarization, but also because of the possibilities either of synergistic inhibitory effects on hERG/I_{Kr} or of raised ivabradine levels in a setting where its metabolism is impaired as a consequence of co-administration of drugs that influence its metabolic pathway. Consistent with these possibilities, in 1 recent report a 68-year-old man receiving ivabradine for paroxysmal sinus tachycardia developed TdP after azithromycin was co-administered to treat acute sinusitis.[9] This patient also had a prolonged QT_c interval during a prior medical examination; TdP did not recur once azithromycin was discontinued.[9] In a second report, an 80-year-old woman receiving multiple medications for unstable angina, including ivabradine, ranolazine, and diltiazem, developed slow junctional rate, prolonged QT_c, and transient TdP.[10] Electrolyte levels were normal and QT_c normalized once ivabradine and diltiazem were discontinued. The authors highlighted that metabolism of ivabradine (and ranolazine) might have been increased as a consequence of CYP 3A inhibition by diltiazem.[10] Potentially, effects of ivabradine on repolarization could be exacerbated in a setting of impaired repolarization reserve,[13] a possibility that merits direct examination in heart failure models.

Comparison of hERG and HCN Channel Block by Ivabradine

A striking feature of the present study is the similarity between ivabradine inhibition of hERG and that of native I_f and recombinant HCN channels, both in blocking potency (Table S1) and in mechanism of inhibition. In particular, the drug has been reported to inhibit HCN4 channels, the dominant HCN isoform in sinoatrial nodal I_f, with an IC_{50} of 2.0 to 2.1 μmol/L,[42,43] very close to the hERG IC_{50} values in Figure 1. Ivabradine inhibits HCN1 either in the closed state or in a transitional state between closed and open, and the direction of current flow has little effect on block.[43] By contrast, for both native I_f and HCN4 channels, block occurs to open channels and is strengthened by depolarization and relieved on hyperpolarization, coupled to inward ion flow.[43,44] The voltage dependence and "envelope of tails" data in this study indicate that hERG block by ivabradine requires channel gating to occur, with a comparatively modest impact on inhibition of inactivation attenuation, consistent with preferential open (activated) channel block. Additionally, although alteration of $[K^+]_e$ from 4 to 2 mmol/L did not influence ivabradine block of outward I_{hERG}, when the direction of K^+ flux was reversed in high $[K^+]_e$, inhibition of inward I_{hERG} was somewhat attenuated (Figure 6), which parallels the effect of inward ion flux on HCN4 block.[43] The hERG channel lacks an S6 proline (P-X-P) motif that restricts the inner cavity size in other K^+ channels, and this may enable it to accommodate a range of drug molecule sizes.[12,45] HCN4 also possesses a comparatively wide pore cavity, which enables ivabradine trapping in the closed configuration.[42] The modest effect of the hERG S624A mutation (Figure 6) and lack of close proximity of the drug to S624 in docking simulations (Figure 7) are consistent with an indirect role for this residue in ivabradine binding to hERG.[23] Sequence alignment of HCN4 and hERG (Figure 7D) shows tyrosine (Y) residues at homologous positions (Y652 hERG; Y506 HCN4) and proximate phenylalanine residues (F656 hERG; F509 HCN4), though HCN4 has an isoleucine at the homologous position (I510) of F656. The Y506A, F509A, and I510A mutations have been shown to impair markedly

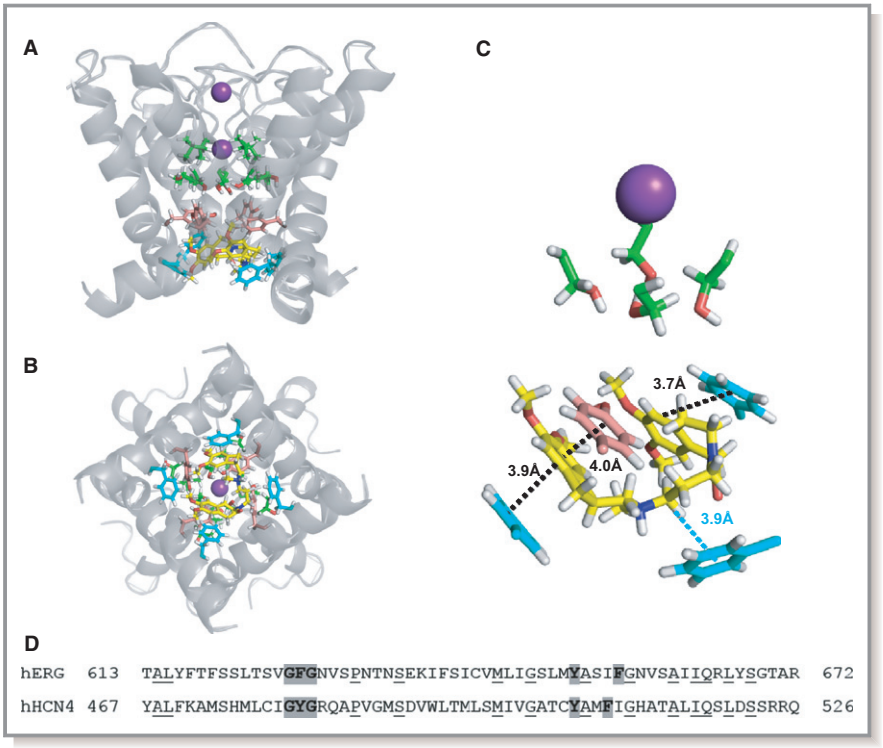

Figure 7. Docking simulation. Lateral (A) and intracellular (B) views of a representative pose for ivabradine docked to the MthK-based human Ether-à-go-go-Related Gene (hERG) open-state homology model. Pore and S6 helices are represented as faint gray ribbon. S624, T623, and V625 pore helical residues are represented as green sticks, while Y652 and F656 are represented respectively as pink and blue sticks. Ivabradine is shown in yellow, while the purple spheres represent the K^+ ions (displayed at full ionic diameter) in positions S1 and S3 of the channel selectivity filter. C, Representative GOLD low-energy score pose for ivabradine docked to the MthK-based model. The side chains of the aromatic residues that make π-π (black dotted line) and cation-π (blue dotted line) interactions with the drug molecule are represented in light blue and pink sticks. The S624 side chains are also shown as green sticks. The potassium ion in the S3 site of the selectivity filter is shown as a purple sphere. The interactions shown include the following: π-π interaction 4.0 Å with Y652; π-π interaction 3.9 Å with F656; π-π interaction 3.7 Å with F656; and π-cation interaction 3.9 Å with F656. For clarity, only the Y652 and F656 residues that make interactions with ivabradine are shown. D, Sequence alignment between hERG and HCN4, focusing on pore helical region/selectivity filter (the GFG and GYG sequences for hERG and HCN4 are shaded) and on the S6 domain for which Y652 and F656 in hERG are shaded and corresponding aromatic residues in HCN4 are also shaded.

ivabradine inhibition of HCN4, with docking simulations to open WT HCN4 channels identifying the drug adopting a bent configuration and stacking interactions between the benzazepinone and benzocylobutane moieties of the drug and Y506 and F509 aromatic side chains.[42] Hydrophobic interactions between I510 and Y506 influence the orientation of Y506 toward the center of the closed channel pore.[42] Both Y652A and F656A mutations greatly attenuate hERG block by ivabradine (Figure 6). The folded compact conformation adopted by ivabradine in our hERG docking simulations allowed the 2 aromatic rings to form multiple π-π interactions with the aromatic side chains of both Y652 and F656, thus mirroring reported docking observations for open WT HCN4.[42]

Thus, our findings provide molecular insight into why ivabradine has a similar potency for hERG as it does for HCN4. However, we do not exclude the possibility that other shared, but yet to be identified, features (eg, lipid association near the channel pore) may also contribute to the similar ivabradine potency against the 2 channels.

Limitations

This study combines data from in vitro experiments on recombinant human (hERG) potassium channels with ventricular repolarization data from perfused hearts from an animal model. The use of intact perfused guinea-pig hearts enabled

effects of ivabradine on both apical and basal ventricular MAPD to be assessed, as well as drug effects on electrical restitution and effective refractory period to be established. Although such experiments are not possible to perform on isolated healthy human hearts and so require approaches such as those adopted here, data from animal models must be extrapolated to humans with caution. For example, the pacing rate cycle length used in this study is somewhat faster than would occur at human resting heart rates. The preparation also shares limitations common to ex vivo preparations that are removed from the normal hormonal and autonomic influences present in vivo. It is noteworthy, however, that in a previous investigation of the utility of guinea-pig paced Langendorff perfused hearts for assessing cardiovascular liability of drugs, 81% (17 of 21) of drugs associated with QT prolongation in the clinic were correctly identified in the guinea-pig perfused heart model,[46] suggestive that this approach is largely reliable. Additionally, the results of our perfused heart experiments in respect of repolarization and restitution can most usefully be considered alongside I_{hERG} IC_{50} data and estimated safety margin[40] in attempting to gauge safety/risk. Another potential limitation of our experiments was the inability to study ivabradine concentrations higher than 0.5 μmol/L in perfused hearts due to sinus arrest. Some other previous studies have not observed sinus arrest at higher ivabradine concentrations.[47–49] However, the use of different species (rabbit,[47] mouse[48]), experimental solutions (in both[47,48]), or preparations (a reduced guinea-pig atrial preparation in[49] as opposed to intact heart) precludes direct comparison with our study.

Conclusions

Ivabradine prolongs ventricular repolarization and alters electrical restitution properties in perfused guinea-pig hearts. hERG/I_{Kr} channel blockade by ivabradine has the potential to contribute to the overall actions of the drug at some plasma concentrations, with tissue accumulation or with impaired repolarization reserve. Ivabradine shows poor pharmacological selectivity between hERG and HCN channels: our data indicate that ivabradine is similarly potent against hERG as reported previously for HCN4, and there are close similarities in blocking mechanism/binding determinants for the 2 channels.[42] This has implications for the future design of HCN-selective bradycardic agents based on an ivabradine-like template.

Sources of Funding

The authors thank the British Heart Foundation for funding (PG/10/96/28661; FS/11/59/28938 [Melgari]; FS/12/2/29300 [Brack]; PG/12/69/29784; PG/11/38/28886).

Disclosures

None.

References

1. Rushworth GF, Lambrakis P, Leslie SJ. Ivabradine: a new rate-limiting therapy for coronary artery disease and heart failure. *Ther Adv Drug Saf*. 2011;2:19–28.
2. Scicchitano P, Cortese F, Ricci G, Carbonara S, Moncelli M, Iacoviello M, Cecere A, Gesualdo M, Zito A, Caldarola P, Scrutinio D, Lagioia R, Riccioni G, Ciccone MM. Ivabradine, coronary artery disease, and heart failure: beyond rhythm control. *Drug Des Devel Ther*. 2014;8:689–700.
3. Savelieva I, Camm AJ. Novel I_f current inhibitor ivabradine: safety considerations. *Adv Cardiol*. 2006;43:79–96.
4. Bois P, Guinamard R, Chemaly AE, Faivre JF, Bescond J. Molecular regulation and pharmacology of pacemaker channels. *Curr Pharm Des*. 2007;13:2338–2349.
5. Bois P, Bescond J, Renaudon B, Lenfant J. Mode of action of bradycardic agent, S 16257, on ionic currents of rabbit sinoatrial node cells. *Br J Pharmacol*. 1996;118:1051–1057.
6. Camm AJ, Lau CP. Electrophysiological effects of a single intravenous administration of ivabradine (S 16257) in adult patients with normal baseline electrophysiology. *Drugs R D*. 2003;4:83–89.
7. Fox K, Ford I, Steg PG, Tardif JC, Tendera M, Ferrari R. Ivabradine in stable coronary artery disease without clinical heart failure. *N Engl J Med*. 2014;371:1091–1099.
8. Martin RI, Pogoryelova O, Santibanez KM, Bourke JP, Teare MD, Keavney BD. Atrial fibrillation associated with ivabradine treatment: meta-analysis of randomised controlled trials. *Heart*. 2014;100:1506–1510.
9. Cocco G, Jerie P. Torsades de pointes induced by the concomitant use of ivabradine and azithromycin: an unexpected dangerous interaction. *Cardiovasc Toxicol*. 2015;15:104–106.
10. Mittal SR. Slow junctional rhythm, QTc prolongation and transient torsades de-pointes following combined use of Ivabradine, Diltiazem and Ranolazine. *J Assoc Physicians India*. 2014;62:426–427.
11. Zeltser D, Justo D, Halkin A, Prokhorov V, Heller K, Viskin S. Torsade de pointes due to noncardiac drugs: most patients have easily identifiable risk factors. *Medicine (Baltimore)*. 2003;82:282–290.
12. Hancox JC, McPate MJ, El Harchi A, Zhang YH. The hERG potassium channel and hERG screening for drug-induced torsades de pointes. *Pharmacol Ther*. 2008;119:118–132.
13. Koncz I, Szel T, Bitay M, Cerbai E, Jaeger K, Fulop F, Jost N, Virag L, Orvos P, Talosi L, Kristof A, Baczko I, Papp JG, Varro A. Electrophysiological effects of ivabradine in dog and human cardiac preparations: potential antiarrhythmic actions. *Eur J Pharmacol*. 2011;668:419–426.
14. Zhou Z, Gong Q, Ye B, Fan Z, Makielski JC, Robertson GA, January CT. Properties of HERG channels stably expressed in HEK 293 cells studied at physiological temperature. *Biophys J*. 1998;74:230–241.
15. Sale H, Wang J, O'Hara TJ, Tester DJ, Phartiyal P, He JQ, Rudy Y, Ackerman MJ, Robertson GA. Physiological properties of hERG 1a/1b heteromeric currents and a hERG 1b-specific mutation associated with Long-QT syndrome. *Circ Res*. 2008;103:e81–e95.
16. Du C, Zhang Y, El Harchi A, Dempsey CE, Hancox JC. Ranolazine inhibition of hERG potassium channels: drug-pore interactions and reduced potency against inactivation mutants. *J Mol Cell Cardiol*. 2014;74:220–230.
17. Milnes JT, Crociani O, Arcangeli A, Hancox JC, Witchel HJ. Blockade of HERG potassium currents by fluvoxamine: incomplete attenuation by S6 mutations at F656 or Y652. *Br J Pharmacol*. 2003;139:887–898.
18. McPate MJ, Duncan RS, Milnes JT, Witchel HJ, Hancox JC. The N588K-HERG K^+ channel mutation in the 'short QT syndrome': mechanism of gain-in-function determined at 37°C. *Biochem Biophys Res Commun*. 2005;334:441–449.
19. El Harchi A, Zhang YH, Hussein L, Dempsey CE, Hancox JC. Molecular determinants of hERG potassium channel inhibition by disopyramide. *J Mol Cell Cardiol*. 2012;52:185–195.
20. McPate MJ, Zhang H, Cordeiro JM, Dempsey CE, Witchel HJ, Hancox JC. hERG1a/1b heteromeric currents exhibit amplified attenuation of inactivation in variant 1 short QT syndrome. *Biochem Biophys Res Commun*. 2009;386:111–117.
21. Du CY, El Harchi A, McPate MJ, Orchard CH, Hancox JC. Enhanced inhibitory effect of acidosis on hERG potassium channels that incorporate the hERG1b isoform. *Biochem Biophys Res Commun*. 2011;405:222–227.

22. Jiang Y, Lee A, Chen J, Cadene M, Chait BT, MacKinnon R. Crystal structure and mechanism of a calcium-gated potassium channel. *Nature*. 2002;417:515–522.
23. Dempsey CE, Wright D, Colenso CK, Sessions RB, Hancox JC. Assessing hERG pore models as templates for drug docking using published experimental constraints: the inactivated state in the context of drug block. *J Chem Inf Model*. 2014;54:601–612.
24. Zhang YH, Colenso CK, Sessions RB, Dempsey CE, Hancox JC. The hERG K^+ channel S4 domain L532P mutation: characterization at 37°C. *Biochim Biophys Acta*. 2011;1808:2477–2487.
25. Jones EM, Roti Roti EC, Wang J, Robertson GA. Cardiac I_{Kr} channels minimally comprise hERG 1a and 1b subunits. *J Biol Chem*. 2004;279:44690–44694.
26. London B, Trudeau MC, Newton KP, Bayer AK, Copeland NG, Gilbert DJ, Jenkins NA, Satler CA, Robertson GA. Two isoforms of the mouse ether-a-go-go related gene coassemble form channels with properties similar to the rapidly activating component of the cardiac delayed rectifier K current. *Circ Res*. 1997;81:870–878.
27. Du CY, Adeniran I, Cheng H, Zhang YH, El Harchi A, McPate MJ, Zhang H, Orchard CH, Hancox JC. Acidosis impairs the protective role of hERG K^+ channels against premature stimulation. *J Cardiovasc Electrophysiol*. 2010;21:1160–1169.
28. Ficker E, Jarolimek W, Kiehn J, Baumann A, Brown AM. Molecular determinants of dofetilide block of HERG K channels. *Circ Res*. 1998;82:386–395.
29. Lees-Miller JP, Duan Y, Teng GQ, Duff HJ. Molecular determinant of high affinity dofetilide binding to HERG1 expressed in Xenopus oocytes: involvement of S6 sites. *Mol Pharmacol*. 2000;57:367–374.
30. Perrin MJ, Kuchel PW, Campbell TJ, Vandenberg JI. Drug binding to the inactivated state is necessary but not sufficient for high-affinity binding to human ether-à-go-go-related gene channels. *Mol Pharmacol*. 2008;74:1443–1452.
31. McPate MJ, Duncan RS, Hancox JC, Witchel HJ. Pharmacology of the short QT syndrome N588K-hERG K^+ channel mutation: differential impact on selected class I and class III antiarrhythmic drugs. *Br J Pharmacol*. 2008;155:957–966.
32. Wolpert C, Schimpf R, Giustetto C, Antzelevitch C, Cordeiro J, Dumaine R, Brugada R, Hong K, Bauersfeld U, Gaita F, Borggrefe M. Further insights into the effect of quinidine in short QT syndrome caused by a mutation in HERG. *J Cardiovasc Electrophysiol*. 2005;16:54–58.
33. Imai YN, Ryu S, Oiki S. Docking model of drug binding to the human ether-a-go-go potassium channel guided by tandem dimer mutant patch-clamp data: a synergic approach. *J Med Chem*. 2009;52:1630–1638.
34. Thollon C, Cambarrat C, Vian J, Prost JF, Peglion JL, Vilaine JP. Electrophysiological effects of S 16257, a novel sino-atrial node modulator, on rabbit and guinea-pig cardiac preparations: comparison with UL-FS 49. *Br J Pharmacol*. 1994;112:37–42.
35. Thollon C, Bidouard JP, Cambarrat C, Lesage L, Reure H, Delescluse I, Vian J, Peglion JL, Vilaine JP. Stereospecific in vitro and in vivo effects of the new sinus node inhibitor (+)-S 16257. *Eur J Pharmacol*. 1997;339:43–51.
36. Joannides R, Moore N, Iacob M, Compagnon P, Lerebours G, Menard JF, Thuillez C. Comparative effects of ivabradine, a selective heart rate-lowering agent, and propranolol on systemic and cardiac haemodynamics at rest and during exercise. *Br J Clin Pharmacol*. 2006;61:127–137.
37. Jiang J, Tian L, Huang Y, Li Y, Xu L. Pharmacokinetic and safety profile of ivabradine in healthy Chinese men: a phase I, randomized, open-label, increasing single- and multiple-dose study. *Clin Ther*. 2013;35:1933–1945.
38. Weiss JN, Chen PS, Qu Z, Karagueuzian HS, Lin SF, Garfinkel A. Electrical restitution and cardiac fibrillation. *J Cardiovasc Electrophysiol*. 2002;13:292–295.
39. Ng GA, Brack KE, Patel VH, Coote JH. Autonomic modulation of electrical restitution, alternans and ventricular fibrillation initiation in the isolated heart. *Cardiovasc Res*. 2007;73:750–760.
40. Redfern WS, Carlsson L, Davis AS, Lynch WG, MacKenzie I, Palethorpe S, Siegl PK, Strang I, Sullivan AT, Wallis R, Camm AJ, Hammond TG. Relationships between preclinical cardiac electrophysiology, clinical QT interval prolongation and torsade de pointes for a broad range of drugs: evidence for a provisional safety margin in drug development. *Cardiovasc Res*. 2003;58:32–45.
41. Jones DK, Liu F, Vaidyanathan R, Eckhardt LL, Trudeau MC, Robertson GA. hERG 1b is critical for human cardiac repolarization. *Proc Natl Acad Sci USA*. 2014;111:18073–18077.
42. Bucchi A, Baruscotti M, Nardini M, Barbuti A, Micheloni S, Bolognesi M, DiFrancesco D. Identification of the molecular site of ivabradine binding to HCN4 channels. *PLoS One*. 2013;8:e53132.
43. Bucchi A, Tognati A, Milanesi R, Baruscotti M, DiFrancesco D. Properties of ivabradine-induced block of HCN1 and HCN4 pacemaker channels. *J Physiol*. 2006;572:335–346.
44. Bucchi A, Baruscotti M, DiFrancesco D. Current-dependent block of rabbit sino-atrial node I_f channels by ivabradine. *J Gen Physiol*. 2002;120:1–13.
45. Mitcheson JS, Chen J, Sanguinetti MC. Trapping of a methanesulfonanilide by closure of the HERG potassium channel activation gate. *J Gen Physiol*. 2000;115:229–240.
46. Guo L, Dong Z, Guthrie H. Validation of a guinea pig Langendorff heart model for assessing potential cardiovascular liability of drug candidates. *J Pharmacol Toxicol Methods*. 2009;60:130–151.
47. Ceconi C, Cargnoni A, Francolini G, Parinello G, Ferrari R. Heart rate reduction with ivabradine improves energy metabolism and mechanical function of isolated ischaemic rabbit heart. *Cardiovasc Res*. 2009;84:72–82.
48. Lauzier B, Vaillant F, Gélinas R, Bouchard B, Brownsey R, Thorin E, Tardif JC, Des Rosiers C. Ivabradine reduces heart rate while preserving metabolic fluxes and energy status of healthy normoxic working hearts. *Am J Physiol Heart Circ Physiol*. 2011;300:H845–H852.
49. Perez O, Gay P, Franqueza L, Carron R, Valenzuela C, Delpon E, Tamargo J. Effects of the two enantiomers, S-16257-2 and S-16260-2, of a new bradycardic agent on guinea-pig isolated cardiac preparations. *Br J Pharmacol*. 1995;115:787–794.

SUPPLEMENTAL MATERIAL

Supplementary Methods

Ventricular pacing

Hearts were paced using a constant current stimulator (SD7A, Digitimer, Welwyn Garden City, UK) delivered through a pacing catheter inserted into the right ventricular (RV) apex at x2 pacing threshold. The effect of ivabradine was investigated during constant right ventricular pacing at 200ms cycle length using 0.2 µM (n=7).

Monophasic action potential duration (APD) restitution

MAPD restitution was studied with right ventricular apical pacing (x2 pacing threshold) using a standard extrastimulus electrical restitution protocol [1-3]. Hearts (n=7) were paced for 25 S_1 beats (200ms CL) followed by an extra-stimulus (S_2) with an initial CL of 200ms. A 10 second rest period in sinus rhythm is allowed before the 26-beat process was repeated at decreasing S_1-S_2 intervals (by 5ms increments until the effective refractory Period (ERP)). ERP is the longest S_1-S_2 interval at which the S_2 beat fails to capture. MAP duration (MAPD) was calculated using a custom made computer program (NewMap, Dr Francis Burton, Glasgow University, UK) at 90% repolarisation ($MAPD_{90}$). Restitution curves were constructed by plotting the S_2-$MAPD_{90}$ against its previous diastolic interval (DI, interval between 90% repolarisation of the 25th S_1MAPD until the activation of the S_2MAPD). An exponential curve function ($MAPD_{90}$ = maximum $MAPD_{90}$ $[1-e^{-DI/\tau}]$), where τ = time constant using Microcal Origin (v 6.0, Origin, San Diego, CA, US) is fitted to this data and the maximum slope of the restitution curve (RT_{max} slope) was obtained from the first derivative of the curve.

Docking of ivabradine to a hERG homology model

The Biopolymer module of Insight II was used to build the ivabradine molecule. The molecule structure was then imported into Sybyl-x 2.0 where the partial charges were calculated using the Gasteiger-Hückel module, and the molecule was energy minimized. The docking was run using

GOLD. In this case the putative binding pocket was defined by a 12 Å radius sphere positioned on the pore axis below the selectivity filter such that all amino acid side chains previously implicated as drug binding determinants were included as potential binding site residues. Side chain flexibility of Y652 and F656 was added to the side chain hydroxyl rotational flexibility of GOLD as described in [4]. 40 separate docking runs incorporating 300,000 generations of the genetic algorithm were made with a total computational time of ≈40 min. GOLD outputs were then ranked using ChemPLP scoring function and the six best conformations were selected for further analysis in Pymol (Schrödinger).

Ivabradine

Ivabradine hydrochloride powder (Sigma) was dissolved in Milli-Q water to produce 1 and 10 mM stock solutions. These stock solutions were diluted in Tyrode at room temperature to obtain the final concentrations reported in the "Results". In experiments on single cells, all the solutions were heated at 37°C and superfused over the cell understudy using a home-made, multi-barrelled superfusion system (<1 s local solution change) [5].

Data Analysis

Data analysis was performed using Clampfit 10.3 (Axon Instruments, now Molecular Devices), Prism v4.03, Prism v5.03 and Excel 2007 and Excel 2013. All data are presented either as the mean ± SEM or as mean with respective 95% Confidence Interval (CI)

The fractional inhibition of I_{hERG} "tail" current by different ivabradine concentrations was determined using the equation:

$$FB = 1 - \frac{I_{hERG-Ivabradine}}{I_{hERG-Control}} \qquad (1)$$

Where $I_{hERG\text{-}Ivabradine}$ and $I_{hERG\text{-}Control}$ represent "tail" currents in the presence or in the absence of a particular concentration of ivabradine. Ivabradine block reached a steady-state within ≈2 minutes and therefore no run-down correction was required.

Concentration-response relations were constructed by plotting mean fractional Inhibition of I_{hERG} tails by different ivabradine concentrations against drug concentration and then fitting the data with a Hill equation in order to obtain the half-maximal inhibitory concentration (IC_{50}) and the Hill coefficient (n_H) values:

$$y = 1/(1 + 10\text{^}((Log\ IC_{50} - x) * n_H)) \qquad (2)$$

Where x is the logarithm of concentration and y is the level of I_{hERG} fractional inhibition at a given concentration and IC_{50} and n_H are as defined above.

The time course of I_{hERG} deactivation was determined by fitting the tail current decay at -40mV following step depolarisation to +20 mV (Figure 1A) with the bi-exponential equation:

$$y = A_s \times \exp(-x/\tau_s) + A_f \times \exp(-x/\tau_f) + C \qquad (3)$$

Where y is I_{hERG} amplitude at time x, τ_s and τ_f are the slow and fast time constant of the two components of the deactivation decay, A_s and A_s are the total current fitted by the fast and the slow component and C is unfitted residual current.

The voltage dependence of activation was studied using the step protocol showed in panels Ai and Aii of Figure S2 and by fitting the normalized tail currents with a Boltzmann equation:

$$I = I_{MAX}/(1 + \exp(V_{0.5} - x/Slope)) \qquad (4)$$

Where I is the tail current amplitude on repolarisation following each depolarising test potential (x), I_{MAX} is the maximal tail current recorded during the protocol, $V_{0.5}$ is the half activation voltage, and '*Slope*' is the slope factor. The same equation was also used to simulate continuous plots (at 2 mV intervals) of voltage-dependent activation of I_{hERG} (Figure 1C).

The time course of I_{hERG} inhibition during using the "envelope of tails" (Figure 4) was determined by calculating fractional block of I_{hERG} tails following each test command and then fitting the resultant data-plot with a single exponential function of the form:

$$Inh = Inh_{MAX} \times (1 - \exp(-K \times x)) \qquad (5)$$

Where Inh is fractional inhibition at time x, and Inh_{max} is the maximal fractional inhibition obtained during the protocol. K is the rate constant of the exponential curve. The time constant was then derived as $1/K$.

The voltage dependence of channel inactivation was established using the three step protocol showed in Figure 5A. The resurgent current at the beginning of the third step was analyzed as described previously [6, 7] and the normalized current has been plotted against the repolarisation potential during the 2ms second step; data were fitted with a Boltzmann equation of the form:

$$I/I_{MAX} = 1 - (1 + exp[(V_{0.5} - V_m)/k]) \qquad (6)$$

Where I is the current amplitude at the beginning of the third step, I_{MAX} is the maximal recorded current after the 2ms step at the testing potential V_m, $V_{0.5}$ is the half-maximal inactivation potential and k is the slope factor for the relationship.

The time-course of I_{hERG} inactivation at +40 mV was calculated by fitting of the resurgent current elicited at +40 mV following a 2ms repolarisation to -120mV with a single exponential equation:

$$y = A \times exp(-x/\tau) + C \qquad (7)$$

Where y is I_{hERG} recorded at time x, τ is the time constant of the decay of the transient current, A represent the total fitted current and C is the residual unfitted current after the decline of the resurgent current.

Results

We investigated reversibility of I_{hERG} block by ivabradine for the highest drug concentration tested (30 µM). Figure S1 shows mean data for the time-course of development of I_{hERG} tail inhibition (Figure S1A) and recovery from inhibition (Figure S1B), assessed during application of the voltage protocol shown in Figure 1 (main text). For each of 5 cells tested, the amplitude of the last I_{hERG} tail elicited in control solution was given a value of 1.0 and then currents during subsequent exposure to and washout from ivabradine were normalized to this. Superfusate was rapidly (<1s) exchanged for ivabradine solution immediately after the last control trace. Current decline was rapid in the

presence of drug (Figure S1A); the data could be fitted with a monoexponential equation, yielding a mean time-constant for block development of 6.5 ± 0.2 s. Figure S1B shows I_{hERG} recovery from inhibition. The last current record in ivabradine (with its tail amplitude expressed as a fraction of control amplitude) was allocated to "0" time, and current amplitude then monitored following superfusate exchange back to control solution. I_{hERG} block was largely, though incompletely reversible over ~3 minutes washout (to 80.7± 3.3% Control), exhibiting a recovery time-constant of 33.8 ± 2.2 s.

I_{hERG} inhibition by ivabradine exhibited some voltage-dependence. Figure S2Ai and Aii contain representative currents at selected voltages during the protocol shown under the traces (test commands were applied in 10 mV increments between -30 and +60 mV). Tail currents were normalized (see Methods) and plotted as shown in Figure S2B, then fitted with equation 4 to derive voltage-dependent activation parameters for I_{hERG}. The control $V_{0.5}$ was -18.15±4.04mV and *k* was 5.82±0.27, whilst in the presence of ivabradine $V_{0.5}$ was -23.25±3.35mV and *k* was 4.78±0.55 (n=5). Thus, ivabradine produced a ~-5.1mV left-shift in voltage-dependent activation. The $V_{0.5}$ and *k* values derived from equation 4 were used to produce continuous plots of voltage-dependent activation in the absence and presence of drug and these were plotted together with voltage-dependence of fractional block of the I_{hERG} tail in Figure S2C and Figure 1C of the main manuscript (*cf* [8]) . The region of voltage-dependence of I_{hERG} tail inhibition coincided closely with the rising phase of the I_{hERG} activation relation, consistent with gating (activation) -dependent block. The small apparent negative fractional block at -30 mV is likely attributable to the impact of the leftward shift in I_{hERG} at this voltage and is reminiscent of that seen with some other hERG channel blocking agents that produce leftward shifted voltage-dependent activation (e.g. [8,9]).

References

1. Brack KE, Coote JH, Ng GA. Vagus nerve stimulation protects against ventricular fibrillation independent of muscarinic receptor activation. *Cardiovasc Res.* 2011;91:437-46.

2. Brack KE, Coote JH, Ng GA. Vagus nerve stimulation inhibits the increase in Ca2+ transient and left ventricular force caused by sympathetic nerve stimulation but has no direct effects alone--epicardial Ca^{2+} fluorescence studies using fura-2 AM in the isolated innervated beating rabbit heart. *Exp Physiol.* 2010;95:80-92.

3. Ng GA, Brack KE, Patel VH, Coote JH. Autonomic modulation of electrical restitution, alternans and ventricular fibrillation initiation in the isolated heart. *Cardiovasc Res.* 2007;73:750-760.

4. Dempsey CE, Wright D, Colenso CK, Sessions RB, Hancox JC. Assessing HERG pore models as templates for drug docking using published experimental constraints: the inactivated state in the context of drug block. *J Chem Inf Model.* 2014;54:601-612.

5. Levi AJ, Hancox JC, Howarth FC, Croker J, Vinnicombe J. A method for making rapid changes of superfusate whilst maintaining temperature at 37^{o}C. *Pflugers Arch.* 1996;432:930-937.

6. McPate MJ, Duncan RS, Milnes JT, Witchel HJ, Hancox JC. The N588K-HERG K^{+} channel mutation in the 'short QT syndrome': mechanism of gain-in-function determined at 37^{o}C. *Biochem Biophys Res Comm.* 2005;334:441-449.

7. Du CY, Adeniran I, Cheng H, Zhang YH, El Harchi A, McPate MJ, Zhang H, Orchard CH, Hancox JC. Acidosis Impairs the protective role of hERG K^{+} Channels against premature stimulation. *J Cardiovasc Electrophysiol.* 2010; 21:1160-1169.

8. Ridley JM, Milnes JT, Zhang YH, Witchel HJ, Hancox JC. Inhibition of HERG K+ current and prolongation of the guinea-pig ventricular action potential by 4-aminopyridine. *J Physiol.* 2003;549:667-672.

9. Ridley JM, Milnes JT, Hancox JC, Witchel HJ. Clemastine, a conventional antihistamine is a high potency inhibitor of the hERG K^{+} channel. *J Mol Cell Cardiol.* 2006;40:107-118.

10. Bucchi A, Baruscotti M, Nardini M, Barbuti A, Micheloni S, Bolognesi M, DiFrancesco D. Identification of the molecular site of ivabradine binding to HCN4 channels. *PLoS One.* 2013;8:e53132.

11. Bois P, Bescond J, Renaudon B, Lenfant J. Mode of action of bradycardic agent, S 16257, on ionic currents of rabbit sinoatrial node cells. *Br J Pharmacol.* 1996;118:1051-1057.

12. Bucchi A, Baruscotti M, DiFrancesco D. Current-dependent block of rabbit sino-atrial node I(f) channels by ivabradine. *J Gen Physiol.* 2002;120:1-13.

13. Bucchi A, Tognati A, Milanesi R, Baruscotti M, DiFrancesco D. Properties of ivabradine-induced block of HCN1 and HCN4 pacemaker channels. *J Physiol.* 2006;572:335-346.

TABLE S1 Comparison of potency of hERG and HCN/I_f channel block by ivabradine

Current	Preparation	IC_{50} (μM)	References
I_{hERG}	HEK 293	2.07	This Study
$I_{hERG\text{-}1a/1b}$	HEK 293	3.31	
I_{hHCN4}	HEK 293	2.1	[10]
I_f	SAN myocytes (rabbit)	2.18	[11]
I_f	SAN myocytes (rabbit)	1.5	[12]
I_{hHCN4}	HEK 293	2.0	[13]
I_{mHCN1}	HEK 293	0.95	

TABLE S2 Effect of ivabradine on electrophysiological properties of the whole heart

	Ivabradine concentration					
	Control	0.1 μM	0.2 μM	0.3 μM	0.4 μM	0.5 μM
HR (bpm)	207.4±9.3	127.9±4.2 [a]	88.4±7.6 [a,b]	64.9±4.4 [a,b]	62.3±5.3 [a,b,c]	63.0±4.9 [a,b]
ERP (ms)	118.0±1.9	129.4±3.0 [a]	142.9±1.6 [a,b]	145.0±2.2 [a,b]	146.7±2.3 [a,b]	145.9±2.0 [a,b]
Base $MAPD_{90max}$ (ms)	117.1±4.3	131.8±2.5 [a]	141.8±2.8 [a]	153.5±0.6 [a,b,c]	153.2±1.2 [a,b,c]	154.9±1.8 [a,b,c]
Apex $MAPD_{90max}$ (ms)	118.6±3.3	136.0±3.4 [a]	139.9±3.6 [a]	144.8±2.0 [a,†]	147.1±3.0 [a,†]	147.7±3.9 [a,†]

Table: Effect of ivabradine on heart rate (HR), effective refractory period (ERP), and maximal monophasic action potential duration at 90% repolarisation ($MAPD_{90max}$) at base and apex regions during electrical restitution. n=7 for all observations. a; $P<0.05$ vs control, b; $P<0.05$ vs 0.1 μM, c; $P<0.05$ vs 0.2 μM repeated measures one way ANOVA, with Bonferroni post-test. [†] $P<0.05$ Apex vs Base $MAPD_{90max}$ (paired t test).

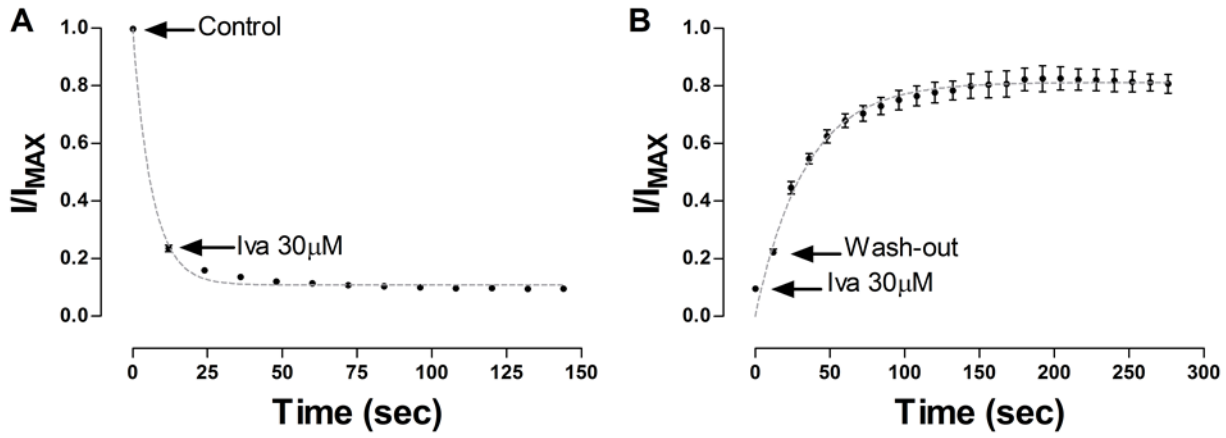

FIGURE S1

A Time course of development of I_{hERG} inhibition by 30 μM ivabradine (n=5). For each cell, the amplitude of I_{hERG} tails at different time points during exposure to ivabradine was normalized to that of the last current in control solution. The arrows highlight the last current in control solution and the first current following rapid superfusate exchange to ivabradine. The fit to the data was made with a monoexponential function with a mean $\tau_{inhibition}$ of 6.5 ± 0.2 s (derived from fits to the data from individual cells).

B Time-course of recovery of I_{hERG} tail current amplitude following washout of 30 μM ivabradine. Tail current amplitudes were expressed as a fraction of control current amplitude prior to ivabradine exposure. The arrows highlight the amplitude of the last current in drug and the first current following washout with control solution. The mean data shown are from 5 cells up to 140 s and 4 cells for the remaining time-points. The fit to the data was with a monoexponential function, yielding a $\tau_{recovery}$ of 33.8 ± 2.2 s (derived from fits to individual cells).

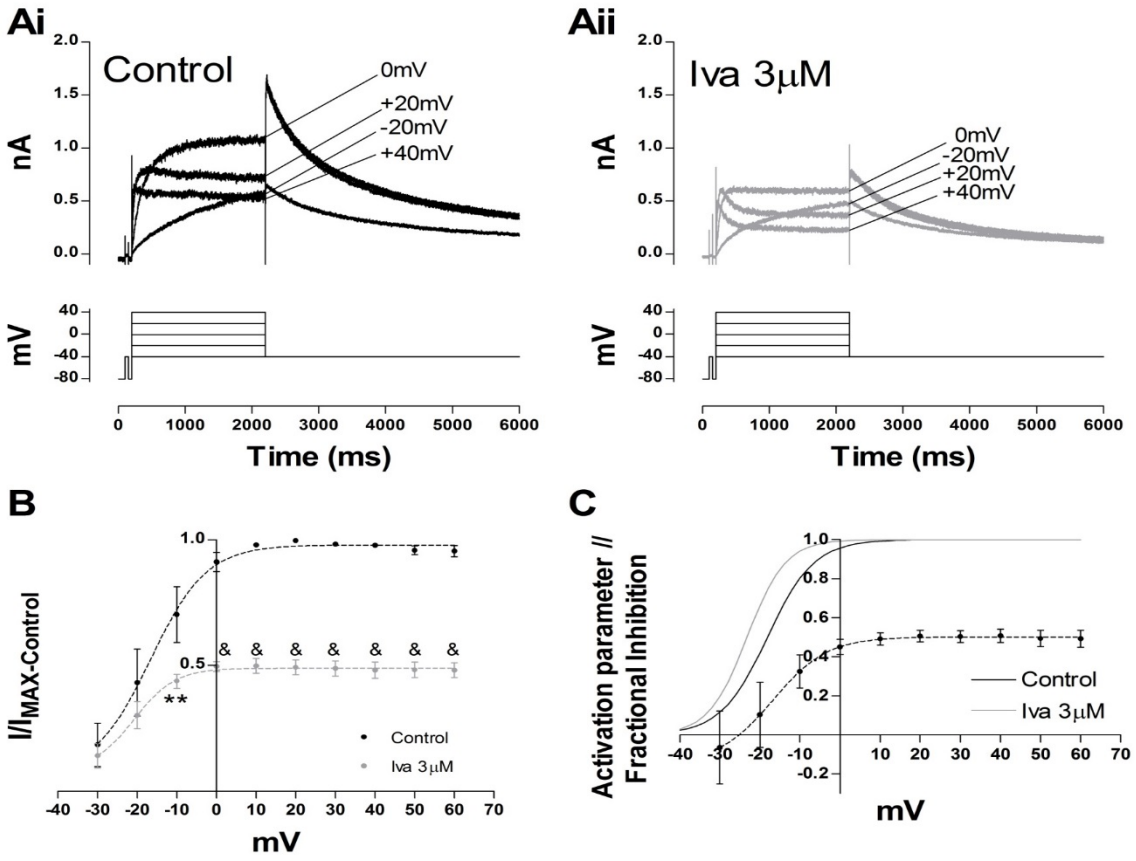

FIGURE S2

A Representative current traces of I_{hERG} elicited by the step protocol showed below in Control (**Ai**) and in presence of 3μM ivabradine (**Aii**; for clarification selected currents at 4 test voltages are shown while the full protocol spanned from -30 to +60mV with a 10mV increase at each step). Peak I_{hERG} tails at -40mV following each depolarising command were measured relative to that elicited by the initial brief 50ms step from -80mV to -40mV.

B Normalised I-V relationship for I_{hERG} tails in Control (black) and in presence of 3μM ivabradine (grey). Peak tail currents in both conditions were normalized to the maximal tail current amplitude recorded in Control (n=5, ******p<0.01 and **&** p<0.001 2-Way ANOVA with Bonferroni post hoc test). The experimental points were fitted with equation 4. Control $V_{0.5}$ = -18.15±4.04mV, Slope 5.82±0.27 and ivabradine 3μM $V_{0.5}$ = -23.25±3.35mV, Slope 4.78±0.55. $V_{0.5}$ p<0.01, Slope ns, paired t-test (n=5).

C Voltage dependence of ivabradine block (black dotted line) and simulated voltage-dependent activation relations for I_{hERG} in Control (black line) and in the presence of 3μM ivabradine. The activation relations were simulated by calculating activation variables at 2 mV intervals using equation 4 and the activation parameters yielded by experimental data. Superimposed is a plot of fractional block against membrane potential (n=5).

hERG Potassium Channel Blockade by the HCN Channel Inhibitor Bradycardic Agent Ivabradine

Dario Melgari, Kieran E. Brack, Chuan Zhang, Yihong Zhang, Aziza El Harchi, John S. Mitcheson, Christopher E. Dempsey, G. André Ng and Jules C. Hancox

J Am Heart Assoc. 2015;4:e001813; originally published April 24, 2015;
doi: 10.1161/JAHA.115.001813
The *Journal of the American Heart Association* is published by the American Heart Association, 7272 Greenville Avenue, Dallas, TX 75231
Online ISSN: 2047-9980

SUPPLEMENTAL MATERIAL

Supplementary Methods

Ventricular pacing

Hearts were paced using a constant current stimulator (SD7A, Digitimer, Welwyn Garden City, UK) delivered through a pacing catheter inserted into the right ventricular (RV) apex at x2 pacing threshold. The effect of ivabradine was investigated during constant right ventricular pacing at 200ms cycle length using 0.2 µM (n=7).

Monophasic action potential duration (APD) restitution

MAPD restitution was studied with right ventricular apical pacing (x2 pacing threshold) using a standard extrastimulus electrical restitution protocol [1-3]. Hearts (n=7) were paced for 25 S_1 beats (200ms CL) followed by an extra-stimulus (S_2) with an initial CL of 200ms. A 10 second rest period in sinus rhythm is allowed before the 26-beat process was repeated at decreasing S_1-S_2 intervals (by 5ms increments until the effective refractory Period (ERP)). ERP is the longest S_1-S_2 interval at which the S_2 beat fails to capture. MAP duration (MAPD) was calculated using a custom made computer program (NewMap, Dr Francis Burton, Glasgow University, UK) at 90% repolarisation ($MAPD_{90}$). Restitution curves were constructed by plotting the S_2-$MAPD_{90}$ against its previous diastolic interval (DI, interval between 90% repolarisation of the 25th S_1MAPD until the activation of the S_2MAPD). An exponential curve function ($MAPD_{90}$ = maximum $MAPD_{90}$ $[1-e^{-DI/\tau}]$), where τ = time constant using Microcal Origin (v 6.0, Origin, San Diego, CA, US) is fitted to this data and the maximum slope of the restitution curve (RT_{max} slope) was obtained from the first derivative of the curve.

Docking of ivabradine to a hERG homology model

The Biopolymer module of Insight II was used to build the ivabradine molecule. The molecule structure was then imported into Sybyl-x 2.0 where the partial charges were calculated using the Gasteiger-Hückel module, and the molecule was energy minimized. The docking was run using

GOLD. In this case the putative binding pocket was defined by a 12 Å radius sphere positioned on the pore axis below the selectivity filter such that all amino acid side chains previously implicated as drug binding determinants were included as potential binding site residues. Side chain flexibility of Y652 and F656 was added to the side chain hydroxyl rotational flexibility of GOLD as described in [4]. 40 separate docking runs incorporating 300,000 generations of the genetic algorithm were made with a total computational time of ≈40 min. GOLD outputs were then ranked using ChemPLP scoring function and the six best conformations were selected for further analysis in Pymol (Schrödinger).

Ivabradine

Ivabradine hydrochloride powder (Sigma) was dissolved in Milli-Q water to produce 1 and 10 mM stock solutions. These stock solutions were diluted in Tyrode at room temperature to obtain the final concentrations reported in the "Results". In experiments on single cells, all the solutions were heated at 37°C and superfused over the cell understudy using a home-made, multi-barrelled superfusion system (<1 s local solution change) [5].

Data Analysis

Data analysis was performed using Clampfit 10.3 (Axon Instruments, now Molecular Devices), Prism v4.03, Prism v5.03 and Excel 2007 and Excel 2013. All data are presented either as the mean ± SEM or as mean with respective 95% Confidence Interval (CI)

The fractional inhibition of I_{hERG} "tail" current by different ivabradine concentrations was determined using the equation:

$$FB = 1 - \frac{I_{hERG-Ivabradine}}{I_{hERG-Control}} \qquad (1)$$

Where $I_{hERG\text{-}Ivabradine}$ and $I_{hERG\text{-}Control}$ represent "tail" currents in the presence or in the absence of a particular concentration of ivabradine. Ivabradine block reached a steady-state within ≈2 minutes and therefore no run-down correction was required.

Concentration-response relations were constructed by plotting mean fractional Inhibition of I_{hERG} tails by different ivabradine concentrations against drug concentration and then fitting the data with a Hill equation in order to obtain the half-maximal inhibitory concentration (IC_{50}) and the Hill coefficient (n_H) values:

$$y = 1/(1 + 10\text{^}((Log\ IC_{50} - x) * n_H)) \qquad (2)$$

Where x is the logarithm of concentration and y is the level of I_{hERG} fractional inhibition at a given concentration and IC_{50} and n_H are as defined above.

The time course of I_{hERG} deactivation was determined by fitting the tail current decay at -40mV following step depolarisation to +20 mV (Figure 1A) with the bi-exponential equation:

$$y = A_s \times \exp(-x/\tau_s) + A_f \times \exp(-x/\tau_f) + C \qquad (3)$$

Where y is I_{hERG} amplitude at time x, τ_s and τ_f are the slow and fast time constant of the two components of the deactivation decay, A_s and A_s are the total current fitted by the fast and the slow component and C is unfitted residual current.

The voltage dependence of activation was studied using the step protocol showed in panels Ai and Aii of Figure S2 and by fitting the normalized tail currents with a Boltzmann equation:

$$I = I_{MAX}/(1 + \exp(V_{0.5} - x/Slope)) \qquad (4)$$

Where I is the tail current amplitude on repolarisation following each depolarising test potential (x), I_{MAX} is the maximal tail current recorded during the protocol, $V_{0.5}$ is the half activation voltage, and '*Slope*' is the slope factor. The same equation was also used to simulate continuous plots (at 2 mV intervals) of voltage-dependent activation of I_{hERG} (Figure 1C).

The time course of I_{hERG} inhibition during using the "envelope of tails" (Figure 4) was determined by calculating fractional block of I_{hERG} tails following each test command and then fitting the resultant data-plot with a single exponential function of the form:

$$Inh = Inh_{MAX} \times (1 - \exp(-K \times x)) \qquad (5)$$

Where Inh is fractional inhibition at time x, and Inh_{max} is the maximal fractional inhibition obtained during the protocol. K is the rate constant of the exponential curve. The time constant was then derived as $1/K$.

The voltage dependence of channel inactivation was established using the three step protocol showed in Figure 5A. The resurgent current at the beginning of the third step was analyzed as described previously [6, 7] and the normalized current has been plotted against the repolarisation potential during the 2ms second step; data were fitted with a Boltzmann equation of the form:

$$I/I_{MAX} = 1 - (1 + exp[(V_{0.5} - V_m)/k]) \qquad (6)$$

Where I is the current amplitude at the beginning of the third step, I_{MAX} is the maximal recorded current after the 2ms step at the testing potential V_m, $V_{0.5}$ is the half-maximal inactivation potential and k is the slope factor for the relationship.

The time-course of I_{hERG} inactivation at +40 mV was calculated by fitting of the resurgent current elicited at +40 mV following a 2ms repolarisation to -120mV with a single exponential equation:

$$y = A \times exp(-x/\tau) + C \qquad (7)$$

Where y is I_{hERG} recorded at time x, τ is the time constant of the decay of the transient current, A represent the total fitted current and C is the residual unfitted current after the decline of the resurgent current.

Results

We investigated reversibility of I_{hERG} block by ivabradine for the highest drug concentration tested (30 µM). Figure S1 shows mean data for the time-course of development of I_{hERG} tail inhibition (Figure S1A) and recovery from inhibition (Figure S1B), assessed during application of the voltage protocol shown in Figure 1 (main text). For each of 5 cells tested, the amplitude of the last I_{hERG} tail elicited in control solution was given a value of 1.0 and then currents during subsequent exposure to and washout from ivabradine were normalized to this. Superfusate was rapidly (<1s) exchanged for ivabradine solution immediately after the last control trace. Current decline was rapid in the

presence of drug (Figure S1A); the data could be fitted with a monoexponential equation, yielding a mean time-constant for block development of 6.5 ± 0.2 s. Figure S1B shows I_{hERG} recovery from inhibition. The last current record in ivabradine (with its tail amplitude expressed as a fraction of control amplitude) was allocated to "0" time, and current amplitude then monitored following superfusate exchange back to control solution. I_{hERG} block was largely, though incompletely reversible over ~3 minutes washout (to 80.7± 3.3% Control), exhibiting a recovery time-constant of 33.8 ± 2.2 s.

I_{hERG} inhibition by ivabradine exhibited some voltage-dependence. Figure S2Ai and Aii contain representative currents at selected voltages during the protocol shown under the traces (test commands were applied in 10 mV increments between -30 and +60 mV). Tail currents were normalized (see Methods) and plotted as shown in Figure S2B, then fitted with equation 4 to derive voltage-dependent activation parameters for I_{hERG}. The control $V_{0.5}$ was -18.15±4.04mV and *k* was 5.82±0.27, whilst in the presence of ivabradine $V_{0.5}$ was -23.25±3.35mV and *k* was 4.78±0.55 (n=5). Thus, ivabradine produced a ~-5.1mV left-shift in voltage-dependent activation. The $V_{0.5}$ and *k* values derived from equation 4 were used to produce continuous plots of voltage-dependent activation in the absence and presence of drug and these were plotted together with voltage-dependence of fractional block of the I_{hERG} tail in Figure S2C and Figure 1C of the main manuscript (*cf* [8]) . The region of voltage-dependence of I_{hERG} tail inhibition coincided closely with the rising phase of the I_{hERG} activation relation, consistent with gating (activation) -dependent block. The small apparent negative fractional block at -30 mV is likely attributable to the impact of the leftward shift in I_{hERG} at this voltage and is reminiscent of that seen with some other hERG channel blocking agents that produce leftward shifted voltage-dependent activation (e.g. [8,9]).

References

1. Brack KE, Coote JH, Ng GA. Vagus nerve stimulation protects against ventricular fibrillation independent of muscarinic receptor activation. *Cardiovasc Res.* 2011;91:437-46.

2. Brack KE, Coote JH, Ng GA. Vagus nerve stimulation inhibits the increase in Ca2+ transient and left ventricular force caused by sympathetic nerve stimulation but has no direct effects alone--epicardial Ca^{2+} fluorescence studies using fura-2 AM in the isolated innervated beating rabbit heart. *Exp Physiol.* 2010;95:80-92.

3. Ng GA, Brack KE, Patel VH, Coote JH. Autonomic modulation of electrical restitution, alternans and ventricular fibrillation initiation in the isolated heart. *Cardiovasc Res.* 2007;73:750-760.

4. Dempsey CE, Wright D, Colenso CK, Sessions RB, Hancox JC. Assessing HERG pore models as templates for drug docking using published experimental constraints: the inactivated state in the context of drug block. *J Chem Inf Model.* 2014;54:601-612.

5. Levi AJ, Hancox JC, Howarth FC, Croker J, Vinnicombe J. A method for making rapid changes of superfusate whilst maintaining temperature at 37^{o}C. *Pflugers Arch.* 1996;432:930-937.

6. McPate MJ, Duncan RS, Milnes JT, Witchel HJ, Hancox JC. The N588K-HERG K^{+} channel mutation in the 'short QT syndrome': mechanism of gain-in-function determined at 37^{o}C. *Biochem Biophys Res Comm.* 2005;334:441-449.

7. Du CY, Adeniran I, Cheng H, Zhang YH, El Harchi A, McPate MJ, Zhang H, Orchard CH, Hancox JC. Acidosis Impairs the protective role of hERG K^{+} Channels against premature stimulation. *J Cardiovasc Electrophysiol.* 2010; 21:1160-1169.

8. Ridley JM, Milnes JT, Zhang YH, Witchel HJ, Hancox JC. Inhibition of HERG K+ current and prolongation of the guinea-pig ventricular action potential by 4-aminopyridine. *J Physiol.* 2003;549:667-672.

9. Ridley JM, Milnes JT, Hancox JC, Witchel HJ. Clemastine, a conventional antihistamine is a high potency inhibitor of the hERG K^{+} channel. *J Mol Cell Cardiol.* 2006;40:107-118.

10. Bucchi A, Baruscotti M, Nardini M, Barbuti A, Micheloni S, Bolognesi M, DiFrancesco D. Identification of the molecular site of ivabradine binding to HCN4 channels. *PLoS One.* 2013;8:e53132.

11. Bois P, Bescond J, Renaudon B, Lenfant J. Mode of action of bradycardic agent, S 16257, on ionic currents of rabbit sinoatrial node cells. *Br J Pharmacol.* 1996;118:1051-1057.

12. Bucchi A, Baruscotti M, DiFrancesco D. Current-dependent block of rabbit sino-atrial node I(f) channels by ivabradine. *J Gen Physiol.* 2002;120:1-13.

13. Bucchi A, Tognati A, Milanesi R, Baruscotti M, DiFrancesco D. Properties of ivabradine-induced block of HCN1 and HCN4 pacemaker channels. *J Physiol.* 2006;572:335-346.

TABLE S1 Comparison of potency of hERG and HCN/I_f channel block by ivabradine

Current	Preparation	IC_{50} (μM)	References
I_{hERG}	HEK 293	2.07	This Study
$I_{hERG\text{-}1a/1b}$	HEK 293	3.31	
I_{hHCN4}	HEK 293	2.1	[10]
I_f	SAN myocytes (rabbit)	2.18	[11]
I_f	SAN myocytes (rabbit)	1.5	[12]
I_{hHCN4}	HEK 293	2.0	[13]
I_{mHCN1}	HEK 293	0.95	

TABLE S2 Effect of ivabradine on electrophysiological properties of the whole heart

	Ivabradine concentration					
	Control	0.1 μM	0.2 μM	0.3 μM	0.4 μM	0.5 μM
HR (bpm)	207.4±9.3	127.9±4.2 [a]	88.4±7.6 [a,b]	64.9±4.4 [a,b]	62.3±5.3 [a,b,c]	63.0±4.9 [a,b]
ERP (ms)	118.0±1.9	129.4±3.0 [a]	142.9±1.6 [a,b]	145.0±2.2 [a,b]	146.7±2.3 [a,b]	145.9±2.0 [a,b]
Base $MAPD_{90max}$ (ms)	117.1±4.3	131.8±2.5 [a]	141.8±2.8 [a]	153.5±0.6 [a,b,c]	153.2±1.2 [a,b,c]	154.9±1.8 [a,b,c]
Apex $MAPD_{90max}$ (ms)	118.6±3.3	136.0±3.4 [a]	139.9±3.6 [a]	144.8±2.0 [a,†]	147.1±3.0 [a,†]	147.7±3.9 [a,†]

Table: Effect of ivabradine on heart rate (HR), effective refractory period (ERP), and maximal monophasic action potential duration at 90% repolarisation ($MAPD_{90max}$) at base and apex regions during electrical restitution. n=7 for all observations. a; $P<0.05$ vs control, b; $P<0.05$ vs 0.1 μM, c; $P<0.05$ vs 0.2 μM repeated measures one way ANOVA, with Bonferroni post-test. [†] $P<0.05$ Apex vs Base $MAPD_{90max}$ (paired t test).

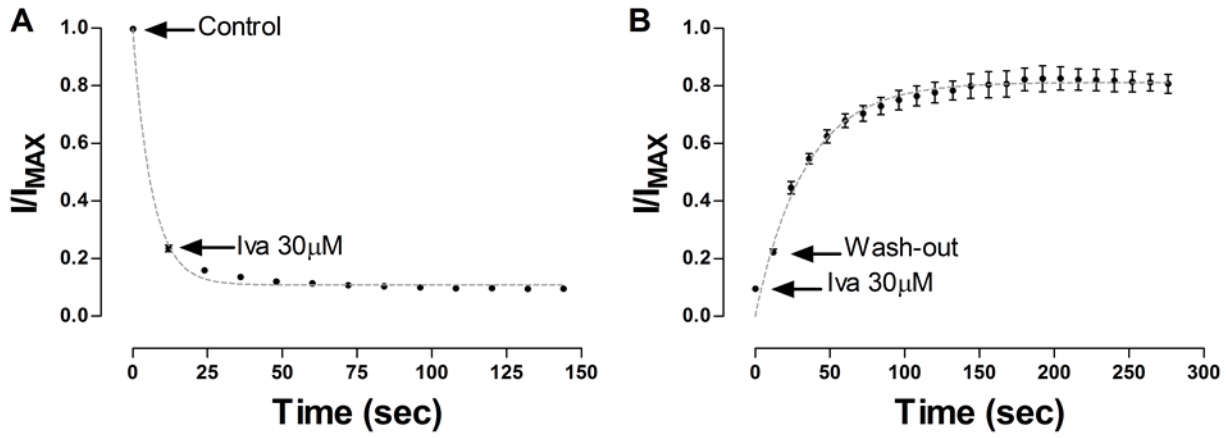

FIGURE S1

A Time course of development of I_{hERG} inhibition by 30 μM ivabradine (n=5). For each cell, the amplitude of I_{hERG} tails at different time points during exposure to ivabradine was normalized to that of the last current in control solution. The arrows highlight the last current in control solution and the first current following rapid superfusate exchange to ivabradine. The fit to the data was made with a monoexponential function with a mean $\tau_{inhibition}$ of 6.5 ± 0.2 s (derived from fits to the data from individual cells).

B Time-course of recovery of I_{hERG} tail current amplitude following washout of 30 μM ivabradine. Tail current amplitudes were expressed as a fraction of control current amplitude prior to ivabradine exposure. The arrows highlight the amplitude of the last current in drug and the first current following washout with control solution. The mean data shown are from 5 cells up to 140 s and 4 cells for the remaining time-points. The fit to the data was with a monoexponential function, yielding a $\tau_{recovery}$ of 33.8 ± 2.2 s (derived from fits to individual cells).

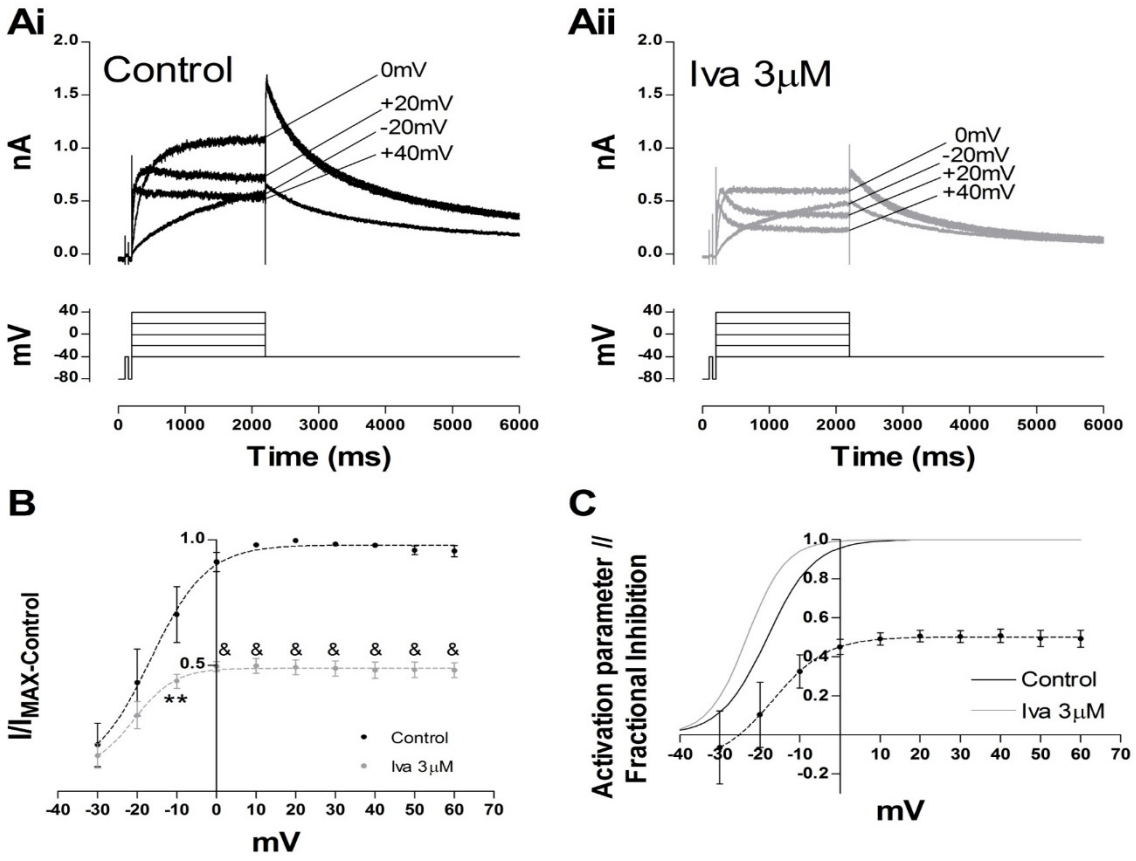

FIGURE S2

A Representative current traces of I_{hERG} elicited by the step protocol showed below in Control (**Ai**) and in presence of 3μM ivabradine (**Aii**; for clarification selected currents at 4 test voltages are shown while the full protocol spanned from -30 to +60mV with a 10mV increase at each step). Peak I_{hERG} tails at -40mV following each depolarising command were measured relative to that elicited by the initial brief 50ms step from -80mV to -40mV.

B Normalised I-V relationship for I_{hERG} tails in Control (black) and in presence of 3μM ivabradine (grey). Peak tail currents in both conditions were normalized to the maximal tail current amplitude recorded in Control (n=5, ******p<0.01 and **&** p<0.001 2-Way ANOVA with Bonferroni post hoc test). The experimental points were fitted with equation 4. Control $V_{0.5}$ = -18.15±4.04mV, Slope 5.82±0.27 and ivabradine 3μM $V_{0.5}$ = -23.25±3.35mV, Slope 4.78±0.55. $V_{0.5}$ p<0.01, Slope ns, paired t-test (n=5).

C Voltage dependence of ivabradine block (black dotted line) and simulated voltage-dependent activation relations for I_{hERG} in Control (black line) and in the presence of 3μM ivabradine. The activation relations were simulated by calculating activation variables at 2 mV intervals using equation 4 and the activation parameters yielded by experimental data. Superimposed is a plot of fractional block against membrane potential (n=5).